

Class Attribute Inference Attacks: Inferring Sensitive Class Information by Diffusion-Based Attribute Manipulations

Your N. Here
Your Institution

Second Name
Second Institution

Abstract

Neural network-based image classifiers are powerful tools for computer vision tasks, but they inadvertently reveal sensitive attribute information about their classes, raising concerns about their privacy. To investigate this privacy leakage, we introduce the first **Class Attribute Inference Attack** (CAIA), which leverages recent advances in text-to-image synthesis to infer sensitive attributes of individual classes in a black-box setting, while remaining competitive with related white-box attacks. Our extensive experiments in the face recognition domain show that CAIA can accurately infer undisclosed sensitive attributes, such as an individual’s hair color, gender, and racial appearance, which are not part of the training labels. Interestingly, we demonstrate that adversarial robust models are even more vulnerable to such privacy leakage than standard models, indicating that a trade-off between robustness and privacy exists.

1 Introduction

Classifying images with neural networks is widely adopted in various domains [4, 5, 10, 22]. Face recognition systems [16], for example, take facial images as input and attempt to predict the depicted person’s identity. In the pursuit of enhancing a model’s predictive performance, privacy concerns of the acquired knowledge are often disregarded and moved into the background. However, correctly assessing and mitigating the risk of compromising private information is crucial in privacy-sensitive domains, as neglect can lead to the disclosure of private information [20, 46, 47]. Face recognition techniques are a fundamental component of many real-life applications, e.g., criminal identification, video surveillance, access control, and autonomous vehicles.

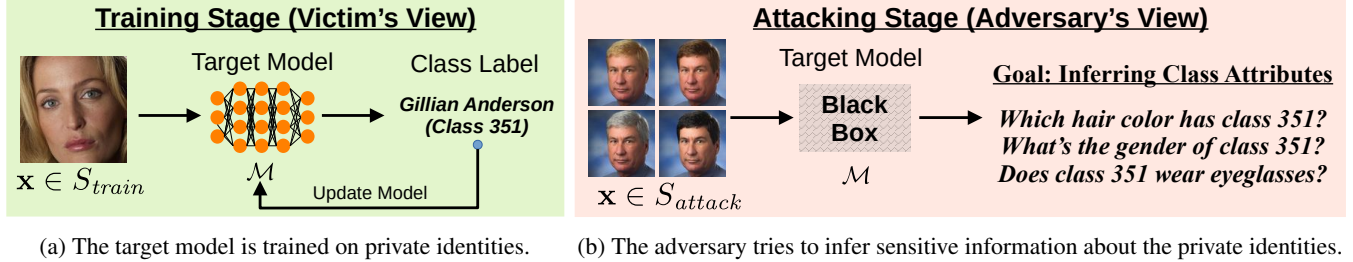
Smart home devices [2], for example, contain face recognition models for access control and user authorization. Users expect these models to recognize them reliably, but at the same time to not reveal information about their appearance to third parties. However, this assumption does not necessarily

hold true, and malicious parties could extract sensitive features about users without any further information about their appearance by simply interacting with the trained classification model in a black-box fashion.

We investigate the privacy leakage of image classifiers and demonstrate that models indeed leak sensitive class information even without any specific information about the classes, training samples, or attribute distributions required by the adversary. We focus our investigation on face recognition models that are trained on labeled datasets where each class corresponds to a different person’s identity. During the training stage, the victim has access to a private dataset of facial images and trains an image classifier on it. After training, the face recognition model makes a prediction on the identity of a given input facial image.

Our research shows that these models reveal sensitive details about the different identities within their outputs, such as gender, hair color, and racial appearance. Fig. 1 illustrates the basic setting of our investigation, in which the adversary has only black-box access to the target model and no specific information about the appearance of individual identities. The goal of the attacking stage is then to infer sensitive information about the individual identities from the training data.

Within our analysis, we introduce a **Class Attribute Inference Attack** (CAIA), which enables an adversary to infer sensitive attributes of a specific class from a trained image classifier with high accuracy. Phrased differently, CAIA allows the creation of a profile of the individual classes by only interacting with the trained classifier through the extraction of class attributes that have not been explicitly part of the training objective. For the attack, we utilize recent advances in text-to-image synthesis to craft images that only differ in one attribute by editing real images with textual guidance. We then exploit that image classifiers, as we show, assign higher logits to inputs that share the same sensitive attribute with the training samples of a class, which allows us to infer class information by only observing the input-output relation of the model.



(a) The target model is trained on private identities. (b) The adversary tries to infer sensitive information about the private identities.

Figure 1: Overview of the setting of our proposed Class Attribute Inference Attack (CAIA). We investigate the setting of face recognition systems, which is a multi-class classification task for which each class corresponds to the identity of an individual. The victim (1a) first trains a model on a private training set S_{train} to predict the identity of a given input image. Whereas the victim has access to a labeled training set and knows all the identities of the training samples, the adversary (1b) only has black-box access to the trained model without any information about the individual classes or training samples. The adversary then tries to infer sensitive attributes about the individual class identities, e.g., their hair color, gender, or racial appearance. For this, the adversary has access to a separate attack dataset S_{attack} of publicly available facial images but has no information about S_{train} .

Compared to related inference attacks [11, 12, 47, 57], CAIA is model-agnostic and requires only black-box access and basic domain knowledge. Once the attack images are crafted, attribute inference requires only a single model forward pass of the generated samples.

In our extensive evaluation, we demonstrate the success of CAIA and show that robust models trained with adversarial training [15, 34] are even more susceptible to these attacks. They leak more information about their individual classes than non-robust models, even if their prediction accuracy is substantially lower. We provide a formal explanation based on the insights that robust models tend to lay their focus on robust image features, which are connected to sensitive attributes. This indicates a trade-off for model designers: making a model robust to adversarial examples comes at the expense of higher privacy leakage.

In summary, we make the following contributions:

- We introduce a novel *Class Attribute Inference Attack* (CAIA) to infer sensitive attributes of specific classes from image classifiers.
- By utilizing recent image manipulation capabilities of diffusion models, CAIA can infer sensitive attributes with high precision.
- We show that robustly-trained models even leak more information, indicating a trade-off between model robustness and privacy leakage.

The paper is structured as follows: We first provide in Sec. 2 an overview of the background and related work, including attribute inference and model inversion attacks. We then introduce the setting and procedure of our Class Attribute Inference Attack (CAIA) in Sec. 3. An extensive experimental evaluation in Sec. 4 demonstrates the strong performance of CAIA and investigates the trade-off between robust models and their privacy leakage. An ablation and

sensitivity analysis concludes our experiments. We discuss our findings together with open challenges in Sec. 5, as well as ethical considerations of our research in Sec. 6. A summary and overview of future avenues conclude the paper in Sec. 7.

Disclaimer: *This paper investigates the extraction of sensitive identity information, including gender and racial appearance of people. The groups used (Asian, Black, Indian, White) are in line with current research and follow the taxonomy of Karkkainen and Joo [27], which itself is adopted from the US Census Bureau [6]. Importantly, we emphasize that this work’s goal is to investigate the leakage of sensitive attributes in image classifiers. We do not intend to discriminate against identity groups or cultures in any way.*

2 Background and Related Work

We start by introducing the background and related work for our analysis. We focus here on attribute inference attacks, which exploit models trained on tabular data to infer hidden attributes for a given input sample, and model inversion attacks, which aim to reconstruct the appearance of training images with the help of generative models. We then highlight the novelty of CAIA compared to existing inference attacks. Furthermore, we present adversarial training to make a model robust against adversarial examples.

2.1 Attribute Inference Attacks

In recent years, various types of inference attacks have been proposed. Those include membership inference attacks [8, 19, 20, 46, 55], which attempt to identify training samples from a larger set of candidates, and property inference attacks [13, 42, 53, 58], which try to infer general properties and statistical information about a model’s training

data. Most related to our work are attribute inference attacks (AIAs) [12], which aim to infer sensitive attribute values of an incomplete data record in the context of classification and regression models. More specifically, the adversary has access to a target model \mathcal{M} , which has been trained on a tabular dataset S_{train} , sampled from the distribution \mathcal{D} . Each training sample is a triplet (x_s, x_n, y) and consists of some sensitive attributes x_s and non-sensitive attributes x_n together with a ground-truth label y . The adversary has access to a set of candidates $(x_n, y) \subseteq S_{train}$ with the sensitive attribute values missing. AIAs try to infer the sensitive values x_s by exploiting \mathcal{M} and its learned information about distribution \mathcal{D} .

Fredrikson et al. [11, 12] proposed maximum-a-posterior AIAs that, assuming all attributes are independent, predict the sensitive attribute value that minimizes the adversary’s expected misclassification rate. Yeom et al. [55] extended the approach and combined attribute inference with membership inference attacks. Mehnaz et al. [35] introduced an attack based on the softmax scores of the target model, assuming that the model’s prediction is more likely to be correct and confident if the input sample contains the true sensitive attribute value. Common AIAs make strong assumptions regarding the adversary’s knowledge that is generally hard to gain under realistic assumptions, e.g., the adversary knows the marginal prior of sample attributes [11, 12, 55] or the target model’s confusion matrix on its training data [11, 35]. Jayaraman and Evans [24] questioned previous black-box AIAs and empirically showed that those attacks could not reveal more private information than a comparable adversary without access to the target model. They conclude that black-box AIAs perform similarly well as data imputation techniques to fill the missing attribute values. To improve AIAs over data imputation, they proposed a white-box attack that outperforms imputation in settings with limited data and skewed distributions.

2.2 Model Inversion Attacks

All presented AIAs are limited to tabular data and are not applicable to image classification since the variation of single image attributes, e.g., changing the hair color in a facial image, is not trivially possible. Moreover, the AIA setting itself is not transferable to the vision domain, since it is unclear how an adversary can have access to incomplete images with only one attribute missing. This fact also makes it impossible to directly compare our *Class Attribute Inference Attack* (CAIA) with common AIAs and corresponding defenses.

Another class of attacks, so-called model inversion attacks (MIAs), try to fill this gap for image classification. We note that the notion of MIAs is not consistent in the literature, and the term is sometimes also used for AIAs. Generally, given a classification model, an adversary attempts to create synthetic input samples that either reconstruct samples from the model’s training data [7, 11, 25, 57] or craft synthetic samples that reflect the characteristics of a specific class [47, 52]. Whereas

most MIAs require access to samples from the target training distribution for training a custom generative adversarial network (GAN), Struppek et al. [47] recently proposed Plug & Play (PPA) MIAs, which make the attacks agnostic to the target model, increase their flexibility, and enhance their inference speed by utilizing pre-trained GANs. We will, therefore, use PPA as a baseline for comparing with our CAIA.

Formally, generative model inversion attacks rely on a generative model $G : W \rightarrow X$, which is trained to map latent vectors $w \in W$ sampled from a probability distribution to the image space X to synthesize facial images. The adversary then optimizes the sampled latent vectors using the target model \mathcal{M} to find meaningful representations of the target identity on the generative model’s learned image manifold. By analyzing the corresponding generated images, the adversary is able to infer sensitive visual features of the individual identities for which \mathcal{M} has been trained to recognize. The optimization goal can be formulated as

$$\min_{\hat{w}} \mathcal{L}(\mathcal{M}(G(\hat{w}), y), \quad (1)$$

which optimizes latent vector \hat{w} for the target class y using a suitable loss function \mathcal{L} . For the optimization, PPA minimizes a Poincaré loss [39] between the generated images and the target identity to overcome the vanishing gradient problem and also performs random transformations on the generated images to avoid overfitting and misleading results. The basic underlying generative model used in PPA is a pre-trained StyleGAN2 [30].

2.3 Novelty of CAIA

In contrast to previous work on AIAs, we move the scope of inference attacks from the sample level to a class level in the vision domain, with the goal of inferring sensitive information about the distinct classes learned by a model. To achieve this, we use the latest advancements in text-to-image synthesis to manipulate single attributes of input images, resulting in consistent images that differ only in the targeted attribute. Our approach is more efficient than MIAs as it requires only black-box access to the target model and no extensive knowledge of the training data distribution. Furthermore, the inference step is done in seconds, since CAIA does not require any further sample optimization after constructing the initial attack dataset. This makes CAIA more flexible and target-independent than previous AIAs and MIAs. Throughout this work, we focus on the privacy-sensitive domain of face recognition systems. The goal is to infer sensitive information about identities, e.g., their gender or racial appearance, without any specific information about the individual identity or underlying training set distributions available to the adversary.

2.4 Adversarial Robust Training

Besides privacy attacks, neural networks are known to be susceptible to adversarial examples [15, 50]. Formally, adversarial examples are crafted by adding an optimized perturbation δ with $\|\delta\| \leq \epsilon$ to a model input x to maximize the model’s loss $\mathcal{L}(\mathcal{M}(x + \delta), y)$ for the true label y . One of the most reliable and commonly used defenses is adversarial training [15, 34], which updates a model’s weights θ on adversarial examples. During each training step, a sample-wise worst-case perturbation is computed in an ϵ -environment around the clean samples to maximize the model’s confusion. These perturbations are then added to the clean samples to train the model and make it robust against such manipulations. Formally, this comes down to a min-max optimization:

$$\min_{\theta} \sum_{(x,y) \in S_{train}} \max_{\|\delta\| \leq \epsilon} \mathcal{L}(\mathcal{M}(x + \delta), y). \quad (2)$$

Since the inner maximization problem cannot be solved numerically in tractable time, local search algorithms are applied to craft adversarial examples, e.g., FGSM [15, 54] or PGD [34]. By training on adversarial examples, the model becomes more robust against adversarial perturbations. In our experiments, we also investigate the influence of model robustness on its privacy leakage.

3 Class Attributes Inference Attacks

We now introduce the novel *Class Attribute Inference Attack* (CAIA), which consists of two steps. First, the adversary generates a set of attack samples by creating different versions of images through a generative approach that alters the sensitive attribute values. In the second step, these attack samples are used to infer the sensitive attribute values for the identities in a face recognition model. The underlying assumption of the attack is that image classifiers assign higher prediction scores to samples that share the sensitive attribute value with the training samples of a class. Before delving into the details, we outline our general threat model.

Adversary’s Goal. Let $\mathcal{M}: X \rightarrow \mathbb{R}^{|Y|}$ denote the trained target image classifier, which takes input images $x \in X$ and computes prediction scores for each class label $y \in Y$. The model’s training data S_{train} consisted of labeled data samples $(x, y) \sim \mathcal{D}$. The underlying attack assumption is that samples of a certain class share a constant sensitive attribute value $z \in Z$, which is not part of the class label but is implicitly encoded in the image features. For example, a face recognition model is a classifier trained to predict the identity y of each facial image x . A sensitive attribute z in this context might be the gender appearance or hair color of a specific identity. The attack goal is to infer the value of this sensitive attribute for each individual class. Fig. 1 demonstrates the general setting, in which the victim trains the target model on labeled

images of various identities. In the depicted case, class y corresponds to the identity of the actress *Gillian Anderson*. The adversary then tries to predict sensitive attributes about the class y without any further information such as the name or training samples of the person’s available. We note that multiple classes can share the same attribute, e.g., having the same hair color.

Adversary’s Capabilities. The adversary has only black-box access to the trained target model \mathcal{M} , i.e., the adversary can query the target model and observe its output logits. Furthermore, the adversary knows the domain of the target model’s training data, e.g., facial images, but not the exact training data distribution or labels. Instead, the adversary can sample images from a data distribution $\hat{\mathcal{D}}$ from the same domain. Note that the images available to the adversary contain no identity labels and have no overlapping with the target models training data. For the sensitive attributes, the adversary defines an individual set of possible values to infer. We emphasize that CAIA is model- and task-agnostic and does not require white-box access to the target model. Information about the prior distribution of the sensitive attributes is neither available nor required.

3.1 Crafting Attack Samples

While it is easy for tabular data to vary the values of attributes in an inference sample, this is a non-trivial task on images since attributes are encoded in pixels, and multiple pixels define not only a single attribute but a set of possibly entangled attributes. For example, human faces contain information such as age and skin color, among many more. Furthermore, changing the value for any of these attributes requires semantically consistent changes in multiple pixels.

To enable meaningful image manipulations, we utilize recent advances in text-to-image synthesis. Recent generative adversarial models (GANs) [14, 29, 30] also offer attribute manipulations by first projecting images into the latent space and then changing the individual latent vector by moving into directions correlated with the target attribute. However, this procedure requires a faithful inversion process to compute the corresponding latent vectors [3, 9, 48] and a preceding analysis of the latent space to discover directions [1, 40, 41] for the desired content changes. Both components are challenging on their own. We, therefore, choose text-guided image synthesis, which allows us to describe desired content changes with natural language and does not require explicit exploration of the latent space.

Text-to-image synthesis systems like Stable Diffusion [44] are able to generate high-quality images following a user-provided text description p . Mokady et al. [36] recently proposed *Null-text Inversion* to encode real images into the domain of diffusion models and enable text-based editing while keeping the overall image composition and content fixed. In

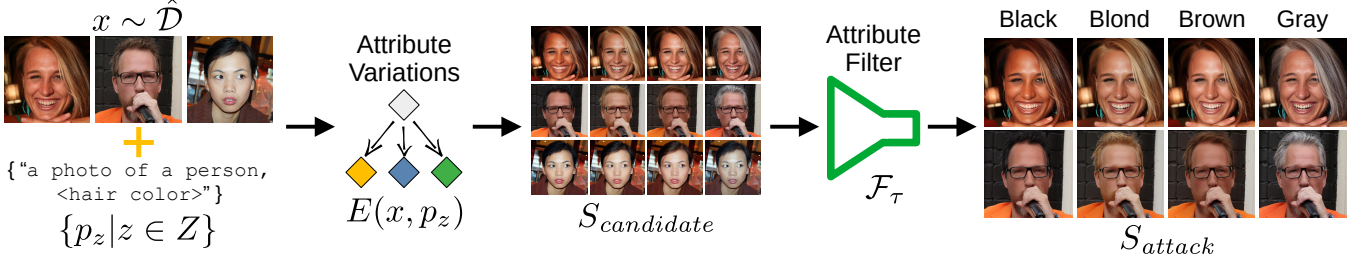


Figure 2: Overview of our attack dataset crafting process for the sensitive attribute *hair color*, which has four possible values. Real images are used to generate image variations by modifying characteristics associated with the sensitive attribute. The resulting candidate images are then filtered to ensure that each sample accurately reflects the intended attribute values. The final output of this process is the set of attack samples.

combination with *Prompt-to-Prompt* [18], it allows a user to instruct image edits $x_{edit} = E(x, p)$ on images x conditioned on a description p . We apply *Null-text Inversion* to generate variations of existing images by changing only the sensitive attribute values, such as the hair color or gender appearance while aiming to leave other image aspects unchanged.

Fig. 2 illustrates the crafting process for the attack samples. Formally, the adversary has access to a data distribution $\hat{\mathcal{D}}$ from which to sample images x . Note that the attack does not require the attack distribution $\hat{\mathcal{D}}$ to be the same as the training data distribution \mathcal{D} but only that both data distributions are from the same domain, e.g., facial images. As we will show in our experimental evaluation, even if the style, size, and quality of images between both distributions vary significantly, the attack is still highly successful.

The adversary defines the target attribute with a set of k possible attribute values $Z = \{z_1, \dots, z_k\}$ and corresponding edit prompts p_z that describe the general domain and explicitly state an attribute value $z \in Z$. For example, $p_z = \text{"A photo of a person, } \langle \text{gender} \rangle\text{"}$, where $\langle \text{gender} \rangle$ is replaced by $z \in \{\text{female appearance, male appearance}\}$. The candidate dataset $S_{candidate}$ is then constructed as

$$S_{candidate} = \{E(x, p_z) | z \in Z, x \sim \hat{\mathcal{D}}\}, \quad (3)$$

consisting of image tuples $\mathbf{x} = (x_1, \dots, x_k)$, each containing k images with different sensitive attribute values.

However, the attribute manipulation might not always succeed in changing an image attribute to the desired value. This can be due to interfering concepts already present in the image that are strongly entangled with the target attribute. For example, changing the hair color of a person with a dark skin tone to blonde often fails because such attribute combinations are rather rare in the actual training data, which is also reflected in the underlying diffusion model. We, therefore, employ a filtering approach, i.e., filtering out all sample tuples \mathbf{x} that are not correctly depicting the various attribute values. For this, we use a trained attribute classifier $\mathcal{F}_\tau: X \rightarrow Z$ to create a subset

$$S_{attack} = \{\mathbf{x} \in S_{candidate} | \mathcal{F}_\tau(x_z) = z, \forall z \in Z\} \quad (4)$$

of sample tuples $\mathbf{x} = (x_1, \dots, x_k)$. The attribute classifier computes for each input image a probability score that the attribute value $z \in Z$ is present in the image. We also add a threshold τ on the softmax scores of the attribute classifier and classify only predictions with a softmax score $\geq \tau$ as correct. This removes images for which the attribute classifier has only low confidence in its prediction. For the example of hair color, each resulting tuple $\mathbf{x} \in S_{attack}$ consists of four facial images (x_1, \dots, x_4) that only differ in the depicted hair color of the person. This use case is also depicted in the attack dataset crafting process in Fig. 2.

3.2 Revealing Sensitive Attributes

After crafting the attack samples, we can now begin inferring the sensitive class attributes learned by the target classifier. We recall that the adversary has no specific information about the distinct classes and particularly no access to the training data samples. Fig. 3 illustrates the basic concept of the inference process. In the depicted case, the adversary tries to infer the sensitive attribute *hair color* of the first identity, which corresponds to the first class of the face recognition model.

While our filtering approach ensures that the variations of an image depict the different values of the sensitive attribute, other confounding behavior might still remain unintentionally. For example, changing a person's hair color to gray might also influence the depicted age. To mitigate such influences, we predict the sensitive attribute with a variety of different attack samples to, in turn, reduce the influence of these confounding factors over a larger number of samples.

Be $\mathcal{M}(x)_y: X \rightarrow \mathbb{R}$ the pre-softmax logits computed by the target model \mathcal{M} on input image x for class y . To infer the sensitive attribute value z of class y , we query the target model consecutively with multiple sample tuples $\mathbf{x} \in S_{attack}$. We then compute for each tuple \mathbf{x} the relative advantage $A(\mathbf{x}) \in \mathbb{R}^{|Z|}$. For each $x_z \in \mathbf{x}$, the relative advantage component $A(\mathbf{x})_z$ is defined by

$$A(\mathbf{x})_z = \max \left(0, \mathcal{M}(x_z)_y - \max_{\tilde{x} \in \mathbf{x}, \tilde{x} \neq x_z} \mathcal{M}(\tilde{x})_y \right). \quad (5)$$

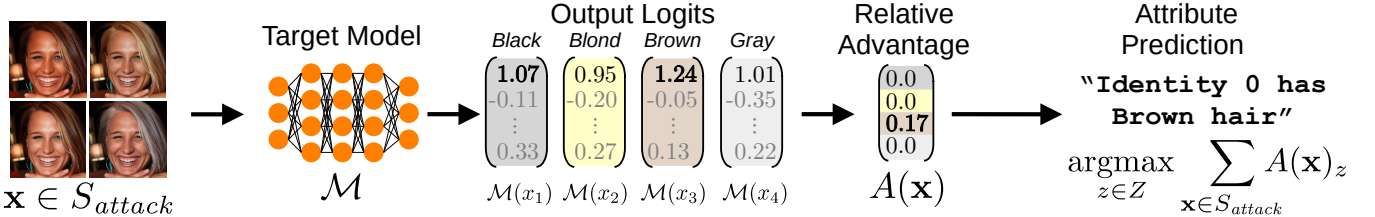


Figure 3: Overview of the class attribute inference step. Each image tuple from the attack set is fed sequentially into the target model to compute the logits for the target class. The relative advantage is then computed by subtracting the second-highest logit value from the maximum value, and this difference is added to a running sum for each sensitive attribute value. The final prediction for the sensitive attribute is the value with the highest relative advantage computed across all attack samples.

The relative advantage computes the difference between the highest and the second-highest logit values and assigns this difference to the attribute sample $x_z \in \mathbf{x}$ with the highest logit. For all other samples $\tilde{x} \in \mathbf{x}$ with $\tilde{x} \neq x_z$, the relative advantage is set to zero. Fig. 3 illustrates the relative advantage computation for a single \mathbf{x} . In the depicted case, the sample depicting *brown hair color* achieves the highest logit value and its relative advantage of $A(\mathbf{x})_{brown} = 0.17$ describes the difference to the second highest logit value assigned to the sample with the attribute *black hair color*. The relative advantage of the other three attribute values is consequently set to zero.

The final attribute prediction \hat{z} is then done by taking the attribute with the highest relative advantage summed up over all attack samples:

$$\hat{z} = \operatorname{argmax}_{z \in Z} \sum_{\mathbf{x} \in S_{attack}} A(\mathbf{x})_z. \quad (6)$$

We emphasize that only a single forward pass on all attack samples is sufficient to compute the relative advantage for all target classes, which makes the inferring step computationally very cheap, e.g., the gender inference for a ResNet-101 model and 500 identities took roughly 2 seconds in our experiments.

4 Experimental Evaluation

Next, we experimentally investigate the information leakage of face recognition models with CAIA. We provide our source code with all hyperparameters to reproduce the experiments and facilitate future research. More experimental details are provided in Appx. A.

4.1 Experimental Setup

Training Datasets. We used the CelebA facial attributes dataset [33] to train our target face recognition systems. CelebA contains labeled images of 10,177 individuals and additional 40 binary attribute annotations per image. We selected the following sensitive attributes:

Attribute	Value	Prompt
Gender	Female	<i>female appearance</i>
	Male	<i>male appearance</i>
Glasses	No Glasses	<i>no eyeglasses</i>
	Glasses	<i>wearing eyeglasses</i>
Racial Appearance	Asian	<i>with asian appearance</i>
	Black	<i>with black skin</i>
	Indian	<i>with indian appearance</i>
	White	<i>with white skin</i>
Hair Color	Black	<i>with black hair</i>
	Blond	<i>with blond hair</i>
	Brown	<i>with brown hair</i>
	Gray	<i>with gray hair</i>

Table 1: Prompts for attack dataset generation. Each prompt is appended to the string "*A photo of a person, < >*" by replacing *< >* with the attribute-specific prompt.

- *gender* = {female, male}
- *eyeglasses* = {no eyeglasses, eyeglasses}
- *hair color* = {black, blond, brown, gray}
- *racial appearance* = {Asian, Black, Indian, White}

For the first three attributes, the CelebA dataset already provides corresponding labels. To infer the attribute *racial appearance*, we applied a pretrained *FairFace* [27] classifier to label each image. Since the provided attributes and labels are often inconsistent for samples of one identity, e.g., people do not always wear eyeglasses or might dye their hair, we created custom subsets for each sensitive attribute group by selecting an equal number of identities for each attribute value and removed samples with inconsistent labels. This is important for evaluation because otherwise the training samples of an identity depict various values for the sensitive attribute, and no clear ground-truth value can be defined.

We trained various target models on these datasets with the standard cross-entropy loss to predict a person’s identity. Note that the attribute labels were not part of the training process. Since not every attribute is present with every identity, we selected the 100 identities for each attribute value of *hair color*, *eyeglasses*, and *racial appearance*, respectively, with the most training samples available. For *gender*, we selected 250 identities per attribute value. We also created larger training datasets with a total of 1,000 identities to see if more identities influence the attack’s success.

Additional target models were trained on the FaceScrub [38] facial image dataset, which contains images of 530 identities with equal gender split. Images are available in a cropped version that only contains a person’s face, and an uncropped version that contains the original image before cropping. Those uncropped images often not only depict a single person but also shows other people in the background which makes training a face recognition system more challenging. We split all datasets into 90% for training and 10% for testing the models’ prediction accuracy. Further details on the different dataset statistics are provided in Appx. A.2.

Attack Datasets. To craft the attack datasets, we used the Flickr-Faces-HQ (FFHQ) [29] and CelebAHQ [28] datasets. Both dataset contain facial images, but compared to CelebA and FaceScrub, these datasets have a much higher resolution, depict a person’s whole head and additional background information. Since the FFHQ dataset consists of images collected from the image hosting platform Flickr, we simulate an adversary who collects samples from public sources, e.g., social media platforms. We then generated and filtered images with attribute manipulations to collect 300 attack image tuples for each attribute group. Tab. 1 states the editing prompts used to manipulate the features of the attack dataset samples. We further set the filter threshold $\tau = 0.6$ in all experiments. We visualize randomly selected training and attack samples in Appx. D.

Training Hyperparameters. We trained ResNet-18, ResNet-101, ResNet-152 [17], ResNeSt-101 [56], and DenseNet169 [21] target models. For each dataset-architecture combination, we trained three models with different seeds. We emphasize that we did not aim for achieving state-of-the-art performances but rather tried to train models with generally good prediction performance.

To investigate the effects of model robustness on information leakage, we trained adversarially robust models on FaceScrub with standard adversarial training [15]. We perturbed training samples with Projected Gradient Descent [34] with 7 steps, $\epsilon = 4/255$, and step size $\alpha = 1/255$ ¹.

We further trained ResNet-50 models on the CelebA attributes for gender, eyeglasses, and hair color for filtering the

candidate images. To mitigate the overconfidence of neural networks, we trained all filter models with label smoothing [37, 51] with a smoothing factor of $\alpha = 0.1$ to calibrate the models and make them more suitable for the confidence threshold filtering. Since some attributes are more frequent in the CelebA dataset, we draw the same number of samples for each attribute value by oversampling/undersampling from the attribute images. To filter images depicting different *racial appearances*, we relied on the pre-trained FairFace classifier. Details on the training of FairFace for filtering the racial appearance images can be found at <https://github.com/dchen236/FairFace>.

We state additional training details, including image preprocessing, augmentation, and optimization parameters in Appx. A.3.

Metrics. We computed the standard classification metrics of precision, recall, and F1 score for each attribute value, together with the overall prediction accuracy for all attributes. All experimental results are averaged over three independently trained models and three disjoint subsets resulting in nine runs per configuration.

Attack Hyperparameters. To create the attack dataset, we first applied Null-Text Inversion [36] with 50 DDIM steps and a guidance scale of 7.5 on Stable Diffusion v1.5². We further used the generic prompt “*A photo of a person*” for all samples. After the inversion, we generated image variations by adding the sensitive attribute values to the prompt using prompt-to-prompt, e.g., “*A photo of a person, female appearance*” and “*A photo of a person, male appearance*” to generate gender variations. See Tab. 1 for all prompts used for generating the different feature representations. For prompt-to-prompt, the cross-replace steps were set to 1.0, and the self-replace steps to 0.4 for gender and eyeglasses and 0.6 for hair color and racial appearance. The confidence threshold for the filter models was set to 0.6 for all models. We then generated and filtered attribute variations one after another until we collected a total of 300 candidates for each attribute category. If not stated otherwise, all attacks were then performed on subsets of 100 candidates.

Baselines. We took random guessing as a naive baseline. Because the sensitive attributes are equally distributed among the different identities, random guessing corresponds to the underlying prior attribute distribution. Since existing AIAs are not applicable to our use case, we instead performed the state-of-the-art Plug & Play model inversion attack (PPA) [47] to synthesize characteristic samples for each class. We then used our filter models to predict the sensitive attribute value for each sample and take the majority vote for each targeted

¹Corresponds to images with pixel values in range [0, 1].

²Available at <https://huggingface.co/runwayml/stable-diffusion-v1-5>.

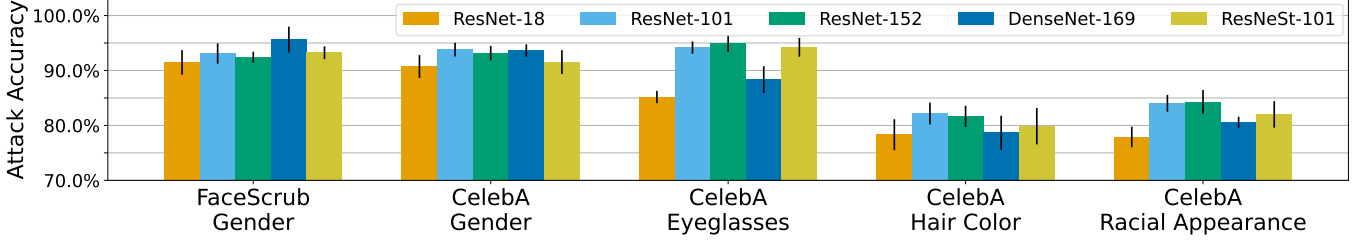


Figure 4: Attack accuracy for different target model architectures and CelebA attribute datasets. Results are averaged over three models and three attack datasets. Except for ResNet-18, the attacks are comparably successful on the different models.

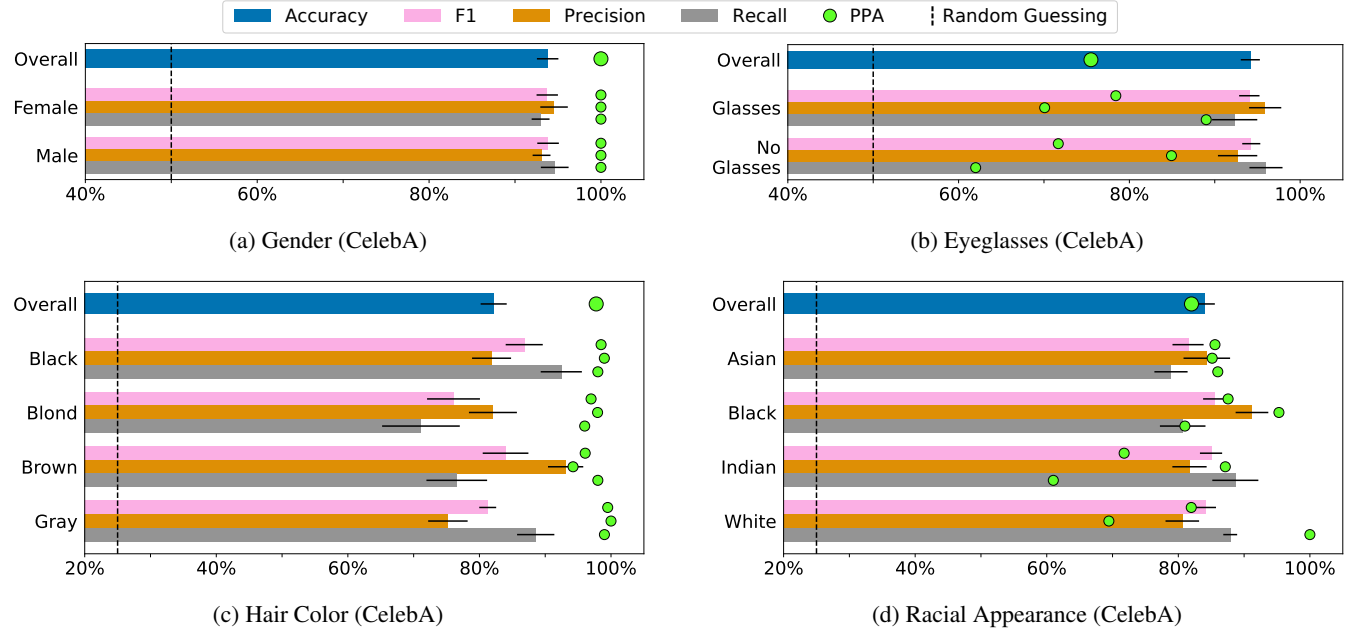


Figure 5: Evaluation results for CAIA performed on ResNet-101 CelebA models to infer four different target attributes. The black horizontal lines denote the standard deviation over nine runs. We further state random guessing (dashed line) and Plug and Play Attacks (PPA, green dots) for comparison. While CAIA outperforms random guessing by a large margin, it extracts information on racial appearance and if someone is wearing eyeglasses even more reliably than the white-box PPA attack.

identity as the attribute prediction. We emphasize that, unlike CAIA, PPA requires white-box access to the target model and a pre-trained GAN, for which we used the official StyleGAN2 [30] FFHQ model. Due to the high computational effort, we limit the PPA comparison to individual ResNet-101 models for each setting. Based on the results stated in the paper [47], we expect PPA to perform comparably on the other architectures.

4.2 Extracting Sensitive Class Information

In the main part of the paper, we focus on results on ResNet-101 models using FFHQ attack samples. We provide more detailed results for the other architectures, CelebAHQ as attack dataset, and experiments with 1,000 target identities in Appx. B. We note that the attack success for an increased

number of identities did not change substantially, even if fewer samples of each identity were available during training. Also, the attack success using CelebAHQ instead of FFHQ as dataset to craft the attack samples has no significant impact on the results and demonstrates that CAIA is not dependent on a specific attack dataset.

The attack accuracy for different models and target attributes in Fig. 4 demonstrates that CAIA performed comparably well on different architectures and predicted the sensitive attribute values correctly in over 90% of the cases for the attributes *gender* and *eyeglasses* and about 80% for the *hair color* and *racial appearance*. Only the attack results of ResNet-18 stand out and are a few percentage points lower than those of the other architectures, which we attribute to the small number of model parameters (only about a quarter of ResNet-101). Still, all attacks reliably inferred the sensitive

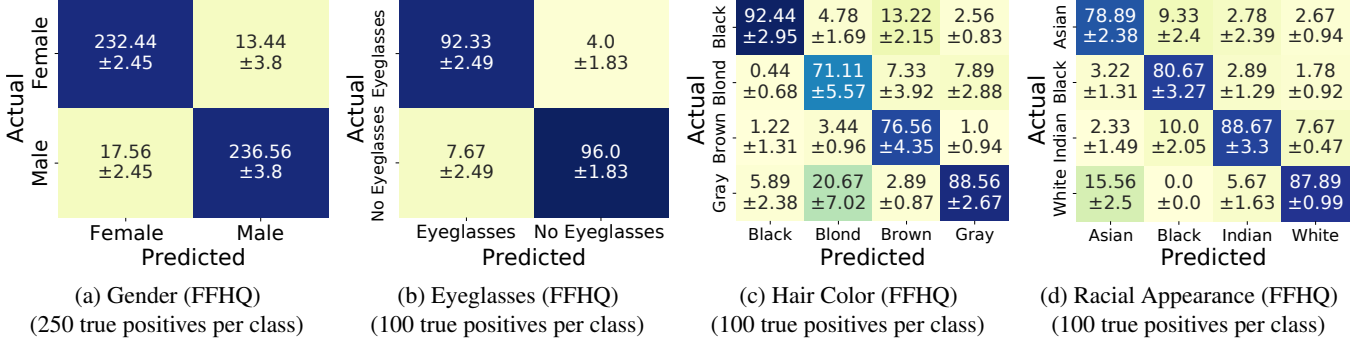


Figure 6: Confusion Matrices for ResNet-101 models trained on the four different CelebA subsets. The results demonstrate that most attribute values can be inferred with similar precision. However, the attacks sometimes tend to falsely predict *blond* hair color as *gray* and *Asian* appearance as *white*.

attributes in most cases.

Next, we investigate the attribute leakage more closely. Therefore, we performed a more detailed analysis of the attribute leakage of ResNet-101 models, for which the results are depicted in Fig. 5. For all four attributes, CAIA significantly beats the random guessing baseline by a large margin. Whereas *gender* and *eyeglasses* were predicted correctly in about 94% of the cases, *racial appearance* could be inferred correctly in 84%. The attack accuracy for *hair color* was also about 82% on average, but the attack success varied substantially between the different attribute values. Fig. 6 shows the confusion matrices for each attribute. For the hair color, blond hair seems to be the hardest value to predict and is frequently confused with gray hair, which is not unexpected since hair colors have different shades, of which blond might be the broadest one. Another reason for the confusion in these attributes is that the CelebA dataset also contains numerous training images of poor quality and sometimes disturbing lighting, which could interfere with the ground-truth identity attributes.

4.3 Comparison with White-Box Attacks

We also investigated gradient-based model inversion attacks, here PPA, to compare to state-of-the-art white-box model inversion methods that reconstruct characteristic class inputs. On the ResNet-101 models, PPA achieved perfect attack results for inferring an identity’s *gender*. It also precisely revealed *hair color* and outperformed the black-box CAIA for both settings. However, for inferring whether an identity is wearing *eyeglasses*, PPA fell significantly behind CAIA. Regarding *racial appearance*, PPA’s attack accuracy was comparable to CAIA but less consistent between different attribute values. We suspect the reason to be the uneven distribution of the *racial appearance* and *eyeglasses* attribute values in the underlying StyleGAN2’s training data [26]. Since PPA starts from randomly sampled latent vectors, the biased attribute distributions also influence the attack’s success in terms of

generating and inferring sensitive attributes. Nevertheless, CAIA shows competitive and impressive performance given that it accesses the target model only in a black-box fashion and has no access to internal gradient information.

4.4 Robustness Increases Privacy Leakage

Since adversarial examples are a common weakness of deep learning models, adversarial training is widely adopted to make models robust against this security threat. To establish a connection between privacy and security, we now extend our investigation to robustly trained models and show that robustness even increases privacy leakage. However, training robust models requires larger datasets due to increased sample complexity [45]. The limited size of the CelebA dataset, which provides approx. 30 samples per identity, makes it difficult to train stable and robust models. Therefore, this section focuses on models trained on FaceScrub, which provides an average of 70 samples per identity and, by this, facilitates stable adversarial training. We trained ResNet-101 models on both cropped images containing only faces and uncropped images, showing a large amount of content unrelated to an identity. For a visual comparison of the datasets, we refer the reader to Appx. D.1.

The attack results for ResNet-101 models are shown in Fig. 7, while Appx. C presents results for other model architectures. Comparing the attack accuracy of non-robust models (93.08%) against that of robust models (96.62%) trained on cropped images suggests that robust models tend to leak more *gender* information about their learned identities than non-robust models, even if the models’ clean prediction accuracy is roughly five percentage points lower. A similar pattern holds for models trained on uncropped images, with robust models still exhibiting higher information leakage. However, it is important to note that the standard model’s prediction accuracy (78.75%) on uncropped images is significantly higher than that of robust models (55.23%). This suggests that a model’s prediction accuracy is not necessarily indicative of

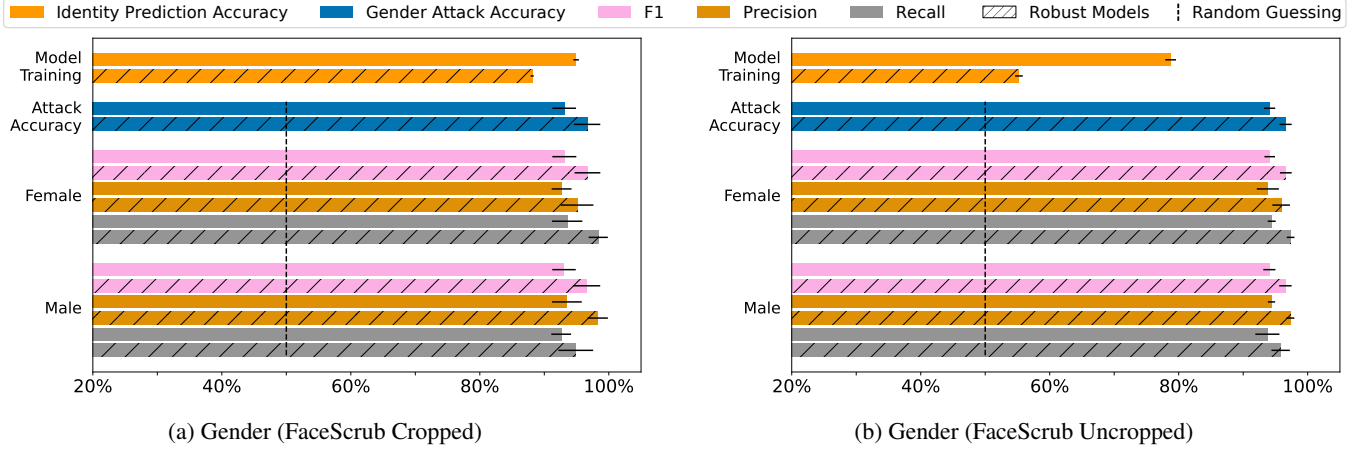


Figure 7: Gender appearance inference results for CAIA performed on ResNet-101 models trained on cropped (a) and uncropped (b) FaceScrub samples. We compared standard models to robust models trained with adversarial training (hatched bars). The results demonstrate that robust models indeed increase the information leakage, even if the underlying models’ prediction accuracy (orange bars) is significantly below that of non-robust models.

its privacy leakage. We hypothesize that robust models tend to exhibit higher privacy leakage due to their concentration on more robust features for their predictions. We formalize and investigate this hypothesis in the remaining section.

Our formal analysis builds upon the robust feature model for binary classifiers of Ilyas et al. [23], which we extend to the privacy leakage setting. Let $\mathcal{M} : X \rightarrow Y$ be a model trained to predict a label $y \in Y$ for each input $x \in X$. We divide a model’s inputs $x = (\tilde{x}, \bar{x})$ into predictive features \tilde{x} and non-predictive features \bar{x} . The i -th predictive feature \tilde{x}^i is positively correlated with a sample’s true label: $E_{(x,y) \sim \mathcal{D}} [\hat{y} \cdot \mathcal{M}(\tilde{x}^i)_y] \geq \rho$ for a sufficiently large ρ . Here, we deviate slightly from our previous notation of y and define $\hat{y} \in \{-1, 1\}$ for each class, with $\hat{y} = 1$ indicating the ground-truth label. We further assume that all model outputs \mathcal{M}_y are centered around zero. Predictive features are (ideally) learned by a model to predict the label. Conversely, a non-predictive feature \bar{x}^j does not correlate with the true label and should be ignored during inference if $E_{(x,y) \sim \mathcal{D}} [\hat{y} \cdot \mathcal{M}(\bar{x}^j)_y] < \rho$.

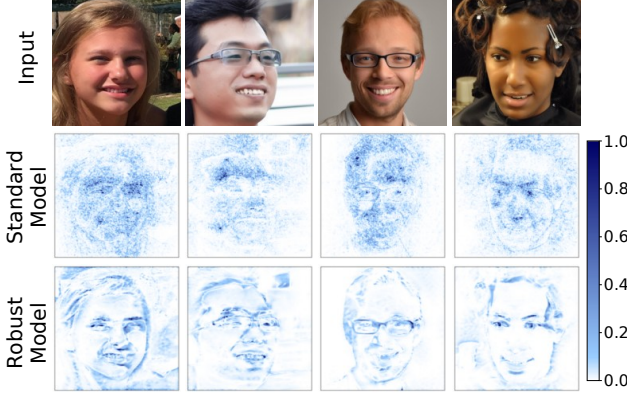
We further explore the nature of the predictive features by categorizing them into two groups: robust features \tilde{x}_{robust} and non-robust features $\tilde{x}_{non-robust}$. Robust predictive features remain predictive even under adversarial perturbations δ with $\|\delta\| \leq \epsilon$, satisfying $E_{(x,y) \sim \mathcal{D}} [\hat{y} \cdot \mathcal{M}(\tilde{x}_{robust} + \delta)_y] \geq \rho$, while non-robust predictive features lose their predictive power under adversarial perturbations. Neural networks rely not only on salient features, such as hair color and other facial characteristics, for image processing, but also on subtle, non-robust image features that can still be highly predictive.

Adversarial perturbations can significantly disrupt non-robust models’ predictions by manipulating $\tilde{x}_{non-robust}$ in an ϵ -environment that is imperceptible to humans. Adversarial training can help reduce the impact of adversarial examples

by focusing the model’s prediction on \tilde{x}_{robust} . However, we stress that adversarial training’s potential to enhance model robustness comes at the cost of increased privacy leakage. To explain why adversarial training increases a model’s privacy leakage, we hypothesize that human-recognizable, sensitive attributes are part of \tilde{x}_{robust} . These attributes are highly predictive because they enable discrimination between samples of different classes based on the assumption that they remain constant within samples of a specific class. We also argue that these attributes are robust features since they are easily identifiable by humans, and small adversarial perturbations are unlikely to affect their value.

In the context of face recognition, *gender* is a sensitive attribute that is highly predictive, enabling us to distinguish individuals from people with other *gender* appearances. Furthermore, it is a robust feature, as altering a person’s *gender* appearance in an image would require significant changes to the pixels. To showcase the importance of robust features in robust models, we utilized the axiomatic attribution method Integrated Gradients [49] on two ResNet-101 models, one trained using standard training and the other with adversarial training. Fig. 8a visualizes the computed gradients for four input images from our attack datasets. While the standard model relies on noisy, non-robust features, such as image background, the robust model concentrates more on human-recognizable facial attributes, including hair, eyes, eyeglasses, and facial structure.

To also provide quantitative support for our analysis, we used Integrated Gradients to measure a model’s relative attribution to specific image parts. For this, we applied a pre-trained face segmentation model [32] to locate various attributes in facial images. Be $H_Z(x) \in \{0, 1\}^{H \times W}$ the binary segmentation mask for image x and attribute class Z , such



(a) Visualized Attribution with Integrated Gradients.

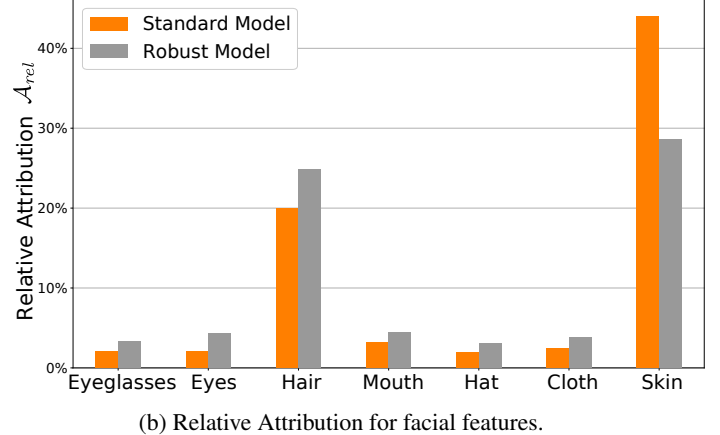


Figure 8: The comparison of absolute attribution based on integrated gradients between a robust and a standard ResNet-101 model in (a) shows that robust models assign perceptually more attuned attribution to facial features. A quantitative comparison of relative attribution in (b) further highlights that the robust model assigns more attribution to unique facial features, such as eyes and hair, while the standard model assigns most attribution to non-specific parts of the skin.

as a person’s hair. Be further $\mathcal{A}(\mathcal{M}, x) \in \mathbb{R}^{H \times W}$ the absolute pixel-wise attribution by Integrated Gradients for model \mathcal{M} and image $x \in \mathbb{R}^{H \times W}$. Let also $\|\cdot\|_1$ denote the sum norm and \odot the Hadamard product. The relative attribution for a dataset X is then computed by:

$$\mathcal{A}_{rel}(\mathcal{M}, X) = \frac{1}{|X|} \sum_{x \in X} \frac{\|\mathcal{A}(\mathcal{M}, x) \odot H_Z(x)\|_1}{\|\mathcal{A}(\mathcal{M}, x)\|_1}. \quad (7)$$

The relative attribution computes the average share of total importance a model assigns to a particular facial attribute.

By analyzing the relative attribution of seven attributes in 100 FFHQ samples and over 530 target identities of ResNet-101 models, Fig. 8b demonstrates that robust models assign more importance to distinct features like eyes or hair, while standard models prioritize general skin areas. This highlights the greater importance placed by robustly trained models on sensitive attributes encoded in images and reflected in their outputs. As CAIA exploits the differences in logits, robust models appear to be more susceptible to such privacy attacks and leak more sensitive attribute information in their outputs. Thus, there exists a trade-off between model robustness and sensitive class information leakage.

[update figure](#)

4.5 Ablation and Sensitivity Analysis

To provide a complete picture of CAIA, we also performed an ablation and sensitivity analysis. We first investigated the influence of the number of attack samples available to the adversary. For this, we repeated the attacks against the ResNet-101 CelebA models and varied the number of attack samples used to compute the relative advantage. As before, results are averaged across three models. We then built nine disjoint attack

datasets for each setting and used three of them for each target model. Our experimental results, which are shown in Fig. 9, demonstrate that 10 to 25 attack samples $\mathbf{x} = (x_1, \dots, x_k)$ are already sufficient to infer the sensitive attributes reliably. Increasing the number any further only improves the results slightly. Even using a single attack example already beats the random guessing baselines significantly. But we also observe a high variance in the results for attacks with only a few attack samples available.

To gain further insights, we selected the attack samples \mathbf{x} that achieved the highest and lowest attack accuracy when performing the attacks only with a single sample. Fig. 10 shows the corresponding images and their achieved attack accuracy for all four attribute settings. The best-performing samples (top row) all clearly portray the different characteristics of the respective target attributes. For example, the *hair color* samples mainly differ in the depicted color of the hair, whereas the face of the woman has barely changed. The samples with the lowest attack accuracy (bottom row) generally have low-quality attribute representations and, in some cases, fail to depict any attribute differences. The results also demonstrate that even if carefully editing the images with *Prompt-to-Prompt* might lead to spurious attribute changes, e.g., removing the eyeglasses could make the person’s appearance more female. Similarly, changing the hair color to gray is also entangled with the perceived age of the depicted person. Future, more reliable synthesis models and image editing techniques will probably overcome such feature entanglements and allow attribute manipulations without introducing unwanted image changes. We expect this to improve the performance of CAIA even further.

We also measured the impact of the filtering approach during the attack dataset synthesis and repeated the process using the FFHQ dataset with two modifications. First, we set the

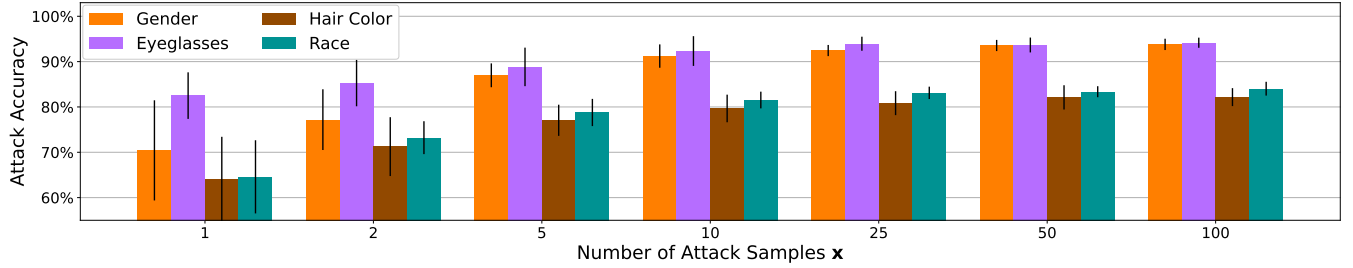


Figure 9: Attack accuracy achieved with a varying number of attack samples x available. Each result has been computed across three ResNet-101 CelebA models and with different subsets of the attack dataset. The results demonstrate that already 10 to 25 attack examples are sufficient to infer the sensitive attributes reliably.

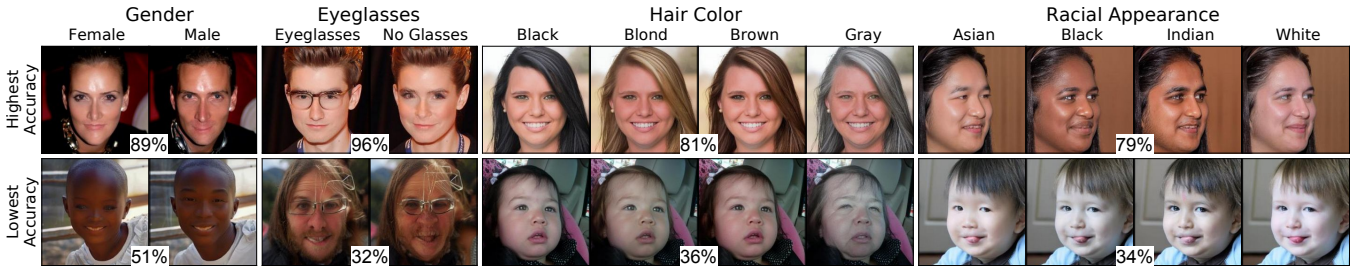


Figure 10: Attack accuracy and illustration of the attack samples x that achieve the highest and lowest accuracy, respectively, on ResNet-101 CelebA models. It becomes clear that samples that represent the different attribute values in a clear way perform best. On the contrary, samples with inconsistent attribute representation are far less informative and fail to extract the sensitive attribute values.

filter threshold to $\tau = 0.0$ and accepted all generated images for which the attribute classifiers predict the target attributes independent of the assigned softmax scores. And second, we completely removed the filtering step and accepted all generated image variations of the first 300 FFHQ samples. We then repeated the attacks on the ResNet-101 CelebA models and compared the results to the ones with the standard filtering approach using a threshold of $\tau = 0.6$ applied. Fig. 11 illustrates the mean attack accuracy for each setting. The results show that the filtering approach significantly improves the attack accuracy for the attributes *Eyeglasses* and *Hair Color*, whereas the accuracy for *Gender* and *Racial Appearance* stays comparable even without any filtering applied. We assume the reason to be that, e.g., adding or removing eyeglasses to a human face is much harder to realize for the generative model than changing a person’s gender appearance. Therefore, the importance of the filter model ensuring that only consistent image variations make it into the attack dataset is higher and has a larger influence on the attack results.

5 Discussion and Challenges

In this paper, we introduced CAIA, a novel privacy attack that enables the inference of sensitive attribute information about classes learned by standard image classifiers. Our extensive experiments demonstrate that classifiers indeed leak

sensitive class information, with significant implications for the secure application of machine learning models. While black-box models have traditionally been practically secure against MIAs and AIAs, our research shows that models in the vision domain are not immune to attribute inference. By leveraging recent advances in text-to-image synthesis, CAIA infers sensitive information from image classifiers with high accuracy, comparable to white-box MIAs. Furthermore, our findings suggest a trade-off between adversarial training and a model’s information leakage, and future adversarial defenses should account for the privacy leakage of models to avoid creating new vulnerabilities.

Although CAIA offers reliable attribute inference capabilities, it still faces some challenges and limitations. Accurately evaluating class information leakage requires high-quality data and consistent labeling, which heavily relies on the underlying dataset. We note that the sample quality of CelebA and FaceScrub images varies widely in terms of resolution, sharpness, and coloring, and the labeling is not always consistent within an identity or attribute class, with also falsely labeled samples contained in the datasets. For instance, the boundaries between gray and blond hair are not well-defined, which can lead to reduced inference accuracy for these attributes. However, CAIA is generally successful in inferring sensitive attribute values in most cases. The attack metrics might even underestimate its effectiveness since false attribute

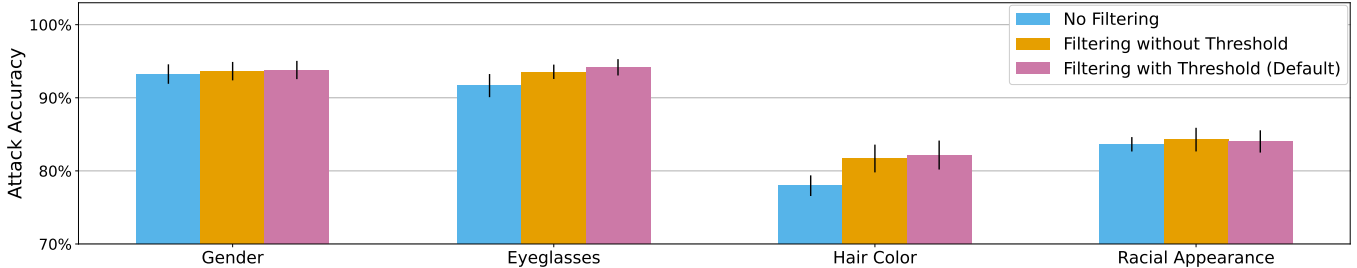


Figure 11: Attack accuracy achieved with unfiltered samples and samples filtered without any confidence threshold compared to our default approach with a confidence threshold of $\tau = 0.6$. The filtering approach mainly improves the results for the attributes *Eyeglasses* and *Hair Color*, and only has a small impact on the attack success for the attributes *Gender* and *Racial Appearance*.

predictions might still provide some identity information, e.g., black skin tone predictions make white as ground truth rather unlikely. Although, the attack may be more powerful for more consistently labeled datasets with higher image quality.

6 Ethical Considerations

Our work demonstrates that common face recognition models leak sensitive information about individuals from the training data. The results of our research might be misused to infer sensitive information through unethical or illegal means. Since face recognition models are already widespread in real-life and privacy-critical applications, e.g., mobile devices, smart home applications, and law enforcement, our proposed Class Attribute Inference Attack (CAIA) could be applied to infer sensitive information from such systems and, therefore, lead to a privacy breach and potential harm to individuals and service providers.

However, we believe it is critical to enhance user awareness and educate practitioners about the existence and feasibility of such attacks. Moreover, CAIA paves the way for future research into the factors facilitating such attacks and the development of potential countermeasures. Understanding such threats enables researchers and service providers to respond early, develop potential security measures, and create more reliable models. These advantages, in our opinion, outweigh any possible concerns. With our research, we also hope to highlight the necessity for users to keep a model’s potential privacy leakage in mind, even if its training data is successfully protected from unauthorized access.

7 Conclusion

To summarize, our research provides novel insights into the privacy of image classifiers and shows that models leak more sensitive information than previously assumed. Our experimental results and formal analysis demonstrate that robust models are particularly susceptible to such attacks, which introduce a novel trade-off between model robustness and privacy. It combines both areas of research, which have largely

been studied separately in previous research. We hope our work motivates future security research and defense endeavors in building secure and private models.

Expanding on the mentioned challenges, we expect that with the upcoming developments in text-guided image manipulation, we propose to enhance CAIA and extend its use to continuous features like age or more detailed skin tone grading. For example, the attack samples could be generated to reflect various shades of dark skin color or fine-grained age representations. Moreover, in its current implementation, CAIA infers each attribute independently. However, in the real world, different attributes often correlate with each other. For example, information inferred on racial appearance influences the probability distribution of hair colors. To this end, CAIA could leverage already inferred attributes as a prior for inferring additional attributes. We also envision the use of CAIA beyond privacy analyses. For example, it is exciting to explore it in the context of explainable AI to determine the importance of features by analyzing prediction scores for different feature characteristics. Similarly, it could be employed to assess the fairness of models and identify potential biases associated with certain classes.

References

- [1] Rameen Abdal, Peihao Zhu, John Femiani, Niloy J. Mitra, and Peter Wonka. Clip2stylegan: Unsupervised extraction of stylegan edit directions. In *Special Interest Group on Computer Graphics and Interactive Techniques Conference (SIGGRAPH)*, pages 48:1–48:9, 2022.
- [2] Adnan Abuassba and Fadi Farha. Access control and authorization in smart homes: A survey. *Tsinghua Science & Technology*, 26:906–917, 2021.
- [3] Yuval Alaluf, Omer Tov, Ron Mokady, Rinon Gal, and Amit Bermano. Hyperstyle: Stylegan inversion with hypernetworks for real image editing. In *Conference on Computer Vision and Pattern Recognition (CVPR)*, pages 18490–18500, 2022.

- [4] Prabal Datta Barua, Nadia Fareeda Muhammad Gowdh, Kartini Rahmat, Norlisah Ramli, Wei Lin Ng, Wai Yee Chan, Mutlu Kuluozturk, Sengul Dogan, Mehmet Baygin, Orhan Yaman, Turker Tuncer, Tao Wen, Kang Hao Cheong, and U. Rajendra Acharya. Automatic covid-19 detection using exemplar hybrid deep features with x-ray images. *International Journal of Environmental Research and Public Health*, 18(15), 2021.
- [5] Ulrich Baumann, Yuan-Yao Huang, Claudius Gläser, Michael Herman, Holger Banzhaf, and J. Marius Zöllner. Classifying road intersections using transfer-learning on a deep neural network. In *International Conference on Intelligent Transportation Systems (ITSC)*, pages 683–690, 2018.
- [6] U.S. Census Bureau. About the topic of race, 2022. URL <https://www.census.gov/topics/population/race/about.html>. Accessed: 22-February-2023.
- [7] Si Chen, Mostafa Kahla, Ruoxi Jia, and Guo-Jun Qi. Knowledge-Enriched Distributional Model Inversion Attacks. In *International Conference on Computer Vision (ICCV)*, pages 16178–16187, 2021.
- [8] Christopher A. Choquette-Choo, Florian Tramèr, Nicholas Carlini, and Nicolas Papernot. Label-only membership inference attacks. In *International Conference on Machine Learning (ICML)*, pages 1964–1974, 2021.
- [9] Tan M. Dinh, Anh Tuan Tran, Rang Nguyen, and Binh-Son Hua. Hyperinverter: Improving stylegan inversion via hypernetwork. In *Conference on Computer Vision and Pattern Recognition (CVPR)*, pages 11379–11388, 2022.
- [10] Andre Esteva, Kat Chou, Serena Yeung, Nikhil Naik, Ali Madani, Ali Mottaghi, Yun Liu, Eric Topol, Jeff Dean, and Richard Socher. Deep learning-enabled medical computer vision. *npj Digital Medicine*, 2021.
- [11] Matt Fredrikson, Somesh Jha, and Thomas Ristenpart. Model Inversion Attacks that Exploit Confidence Information and Basic Countermeasures. In *Conference on Computer and Communications Security (CCS)*, pages 1322–1333, 2015.
- [12] Matthew Fredrikson, Eric Lantz, Somesh Jha, Simon M. Lin, David Page, and Thomas Ristenpart. Privacy in pharmacogenetics: An end-to-end case study of personalized warfarin dosing. In *USENIX Security Symposium*, pages 17–32, 2014.
- [13] Karan Ganju, Qi Wang, Wei Yang, Carl A. Gunter, and Nikita Borisov. Property inference attacks on fully connected neural networks using permutation invariant representations. In *Conference on Computer and Communications Security (CCS)*, pages 619–633, 2018.
- [14] Ian Goodfellow, Jean Pouget-Abadie, Mehdi Mirza, Bing Xu, David Warde-Farley, Sherjil Ozair, Aaron Courville, and Yoshua Bengio. Generative Adversarial Nets. In *Conference on Neural Information Processing Systems (NeurIPS)*, 2014.
- [15] Ian J. Goodfellow, Jonathon Shlens, and Christian Szegedy. Explaining and harnessing adversarial examples. In *International Conference on Learning Representations (ICLR)*, 2015.
- [16] Guodong Guo and Na Zhang. A survey on deep learning based face recognition. *Computer Vision and Image Understanding*, 189, 2019.
- [17] Kaiming He, Xiangyu Zhang, Shaoqing Ren, and Jian Sun. Deep residual learning for image recognition. In *Conference on Computer Vision and Pattern Recognition (CVPR)*, pages 770–778, 2016.
- [18] Amir Hertz, Ron Mokady, Jay Tenenbaum, Kfir Aberman, Yael Pritch, and Daniel Cohen-Or. Prompt-to-prompt image editing with cross attention control. *arXiv preprint*, arXiv:2208.01626, 2022.
- [19] Dominik Hintersdorf, Lukas Struppek, and Kristian Kersting. To trust or not to trust prediction scores for membership inference attacks. In *International Joint Conference on Artificial Intelligence (IJCAI)*, pages 3043–3049, 2022.
- [20] Dominik Hintersdorf, Lukas Struppek, and Kristian Kersting. Clipping privacy: Identity inference attacks on multi-modal machine learning models. *arXiv preprint*, arXiv:2209.07341, 2022.
- [21] Gao Huang, Zhuang Liu, Laurens van der Maaten, and Kilian Q. Weinberger. Densely Connected Convolutional Networks. In *Conference on Computer Vision and Pattern Recognition (CVPR)*, pages 2261–2269, 2017.
- [22] Ahmad Ibrahim, Hoda K. Mohamed, Ali Maher, and Baochang Zhang. A survey on human cancer categorization based on deep learning. *Frontiers in Artificial Intelligence*, 5, 2022.
- [23] Andrew Ilyas, Shibani Santurkar, Dimitris Tsipras, Logan Engstrom, Brandon Tran, and Aleksander Madry. Adversarial examples are not bugs, they are features. In *Conference on Neural Information Processing Systems (NeurIPS)*, volume 32, 2019.

- [24] Bargav Jayaraman and David Evans. Are attribute inference attacks just imputation? In *Conference on Computer and Communications Security (CCS)*, pages 1569–1582, 2022.
- [25] Mostafa Kahla, Si Chen, Hoang Anh Just, and Ruoxi Jia. Label-only model inversion attacks via boundary repulsion. In *Conference on Computer Vision and Pattern Recognition (CVPR)*, pages 15025–15033, 2022.
- [26] Cemre Karakas, Alara Dirik, Eylul Yalcinkaya, and Pinar Yanardag. Fairstyle: Debiasing stylegan2 with style channel manipulations. In *European Conference on Computer Vision (ECCV)*, volume 13673, pages 570–586, 2022.
- [27] Kimmo Karkkainen and Jungseock Joo. Fairface: Face attribute dataset for balanced race, gender, and age for bias measurement and mitigation. In *Winter Conference on Applications of Computer Vision (WACV)*, pages 1548–1558, 2021. Pretrained classifier available at <https://github.com/dchen236/FairFace>.
- [28] Tero Karras, Timo Aila, Samuli Laine, and Jaakko Lehtinen. Progressive growing of gans for improved quality, stability, and variation. In *International Conference on Learning Representations (ICLR)*, 2018.
- [29] Tero Karras, Samuli Laine, and Timo Aila. A Style-Based Generator Architecture for Generative Adversarial Networks. In *Conference on Computer Vision and Pattern Recognition (CVPR)*, pages 4401–4410, 2019.
- [30] Tero Karras, Samuli Laine, Miika Aittala, Janne Hellsten, Jaakko Lehtinen, and Timo Aila. Analyzing and Improving the Image Quality of StyleGAN. In *Conference on Computer Vision and Pattern Recognition (CVPR)*, 2020. Pretrained FFHQ model available at <https://github.com/NVlabs/stylegan2-ada-pytorch>.
- [31] Diederik P. Kingma and Jimmy Ba. Adam: Method for Stochastic Optimization. In *International Conference on Learning Representations (ICLR)*, 2015.
- [32] Cheng-Han Lee, Ziwei Liu, Lingyun Wu, and Ping Luo. Maskgan: Towards diverse and interactive facial image manipulation. In *IEEE Conference on Computer Vision and Pattern Recognition (CVPR)*, 2020. Pre-trained model available at <https://github.com/switchable/norms/CelebAMask-HQ>.
- [33] Ziwei Liu, Ping Luo, Xiaogang Wang, and Xiaoou Tang. Deep Learning Face Attributes in the Wild. In *International Conference on Computer Vision (ICCV)*, 2015.
- [34] Aleksander Madry, Aleksandar Makelov, Ludwig Schmidt, Dimitris Tsipras, and Adrian Vladu. Towards deep learning models resistant to adversarial attacks. In *International Conference on Learning Representations (ICLR)*, 2018.
- [35] Shagufta Mehnaz, Sayanton V. Dibbo, Ehsanul Kabir, Ninghui Li, and Elisa Bertino. Are your sensitive attributes private? novel model inversion attribute inference attacks on classification models. In *USENIX Security Symposium*, pages 4579–4596, 2022.
- [36] Ron Mokady, Amir Hertz, Kfir Aberman, Yael Pritch, and Daniel Cohen-Or. Null-text inversion for editing real images using guided diffusion models. *arXiv preprint*, arXiv:2211.09794, 2022.
- [37] Rafael Müller, Simon Kornblith, and Geoffrey E. Hinton. When does label smoothing help? In *Conference on Neural Information Processing Systems (NeurIPS)*, pages 4696–4705, 2019.
- [38] Hongwei Ng and Stefan Winkler. A data-driven approach to cleaning large face datasets. In *IEEE International Conference on Image Processing (ICIP)*, pages 343–347, 2014.
- [39] Maximilian Nickel and Douwe Kiela. Poincaré Embeddings for Learning Hierarchical Representations. In *Conference on Neural Information Processing Systems (NeurIPS)*, pages 6341–6350, 2017.
- [40] Ehsan Pajouheshgar, Tong Zhang, and Sabine Süsstrunk. Optimizing latent space directions for gan-based local image editing. In *International Conference on Acoustics, Speech and Signal Processing (ICASSP)*, pages 1740–1744, 2022.
- [41] Rishabh Parihar, Ankit Dhiman, Tejan Karmali, and Venkatesh R. Everything is there in latent space: Attribute editing and attribute style manipulation by stylegan latent space exploration. In *ACM International Conference on Multimedia*, pages 1828–1836, 2022.
- [42] Mathias P. M. Parisot, Balázs Pejó, and Dayana Spagnuelo. Property inference attacks on convolutional neural networks: Influence and implications of target model’s complexity. In *International Conference on Security and Cryptography (SECRYPT)*, pages 715–721, 2021.
- [43] Adam Paszke, Sam Gross, Francisco Massa, Adam Lerer, James Bradbury, Gregory Chanan, Trevor Killeen, Zeming Lin, Natalia Gimelshein, Luca Antiga, Alban Desmaison, Andreas Köpf, Edward Yang, Zachary DeVito, Martin Raison, Alykhan Tejani, Sasank Chilamkurthy, Benoit Steiner, Lu Fang, Junjie Bai, and

- Soumith Chintala. PyTorch: An Imperative Style, High-Performance Deep Learning Library. In *Conference on Neural Information Processing Systems (NeurIPS)*, pages 8024–8035, 2019.
- [44] Robin Rombach, Andreas Blattmann, Dominik Lorenz, Patrick Esser, and Björn Ommer. High-resolution image synthesis with latent diffusion models. In *Conference on Computer Vision and Pattern Recognition (CVPR)*, pages 10684–10695, 2022.
- [45] Ludwig Schmidt, Shibani Santurkar, Dimitris Tsipras, Kunal Talwar, and Aleksander Madry. Adversarially robust generalization requires more data. In *Conference on Neural Information Processing Systems (NeurIPS)*, pages 5019–5031, 2018.
- [46] Reza Shokri, Marco Stronati, Congzheng Song, and Vitaly Shmatikov. Membership inference attacks against machine learning models. In *Symposium on Security and Privacy (S&P)*, pages 3–18, 2017.
- [47] Lukas Struppek, Dominik Hintersdorf, Antonio De Almeida Correia, Antonia Adler, and Kristian Kersting. Plug & play attacks: Towards robust and flexible model inversion attacks. In *International Conference on Machine Learning (ICML)*, volume 162, pages 20522–20545, 2022.
- [48] Rakshith Subramanyam, Vivek Sivaraman Narayanaswamy, Mark Naufel, Andreas Spanias, and Jayaraman J. Thiagarajan. Improved stylegan-v2 based inversion for out-of-distribution images. In *International Conference on Machine Learning (ICML)*, volume 162, pages 20625–20639, 2022.
- [49] Mukund Sundararajan, Ankur Taly, and Qiqi Yan. Axiomatic attribution for deep networks. In *International Conference on Machine Learning (ICML)*, volume 70, pages 3319–3328, 2017.
- [50] Christian Szegedy, Wojciech Zaremba, Ilya Sutskever, Joan Bruna, Dumitru Erhan, Ian J. Goodfellow, and Rob Fergus. Intriguing properties of neural networks. In *International Conference on Learning Representations (ICLR)*, 2014.
- [51] Christian Szegedy, Vincent Vanhoucke, Sergey Ioffe, Jonathon Shlens, and Zbigniew Wojna. Rethinking the inception architecture for computer vision. In *Conference on Computer Vision and Pattern Recognition (CVPR)*, pages 2818–2826, 2016.
- [52] Kuan-Chieh Wang, Yan Fu, Ke Liand Ashish Khisti, Richard Zemel, and Alireza Makhzani. Variational Model Inversion Attacks. In *Conference on Neural Information Processing Systems (NeurIPS)*, 2021.
- [53] Xiuling Wang and Wendy Hui Wang. Group property inference attacks against graph neural networks. In *Conference on Computer and Communications Security (CCS)*, pages 2871–2884, 2022.
- [54] Eric Wong, Leslie Rice, and J. Zico Kolter. Fast is better than free: Revisiting adversarial training. In *International Conference on Learning Representations (ICLR)*, 2020.
- [55] Samuel Yeom, Irene Giacomelli, Matt Fredrikson, and Somesh Jha. Privacy risk in machine learning: Analyzing the connection to overfitting. In *Computer Security Foundations Symposium (CSF)*, pages 268–282, 2018.
- [56] Hang Zhang, Chongruo Wu, Zhongyue Zhang, Yi Zhu, Haibin Lin, Zhi Zhang, Yue Sun, Tong He, Jonas Mueller, R. Manmatha, Mu Li, and Alexander Smola. Resnest: Split-attention networks. *CoRR*, abs/2004.08955, 2020.
- [57] Yuheng Zhang, Ruoxi Jia, Hengzhi Pei, Wenxiao Wang, Bo Li, and Dawn Song. The Secret Revealer: Generative Model-Inversion Attacks Against Deep Neural Networks. In *Conference on Computer Vision and Pattern Recognition (CVPR)*, pages 250–258, 2020.
- [58] Junhao Zhou, Yufei Chen, Chao Shen, and Yang Zhang. Property inference attacks against gans. In *Annual Network and Distributed System Security Symposium (NDSS)*, 2022.

A Experimental Details

A.1 Hard- and Software Details

We performed our experiments on NVIDIA DGX machines running NVIDIA DGX Server Version 5.1.0 and Ubuntu 20.04.4 LTS. The machines have 2TB of RAM and contain NVIDIA A100-SXM4-40GB GPUs and AMD EPYC 7742 CPUs. We further relied on CUDA 11.4, Python 3.10.0, and PyTorch 1.12.1 with Torchvision 0.13.1 [43] for our experiments. If not stated otherwise, we used the model architecture implementations and pre-trained ImageNet weights provided by Torchvision. We further provide a Dockerfile together with our code to make the reproduction of our results easier. In addition, all training and attack configuration files are available to reproduce the results stated in this paper.

To perform Plug & Play Attacks (PPA), we used a NVIDIA DGX machine running NVIDIA DGX Server Version 5.2.0 and Ubuntu 20.04.4 LTS. The machines has 2TB of RAM and contain NVIDIA A100-SXM4-80GB GPUs and AMD EPYC 7742 CPUs. The experiments were performed with CUDA 11.4, Python 3.8.10, and PyTorch 1.10.0 with Torchvision 0.11.0. We further used PPA in combination with the pre-trained FFHQ StyleGAN-2 and relied on the standard CelebA attack parameters, as stated in Struppek et al. [47] and <https://github.com/LukasStruppek/Plug-and-Play-Attacks>. We only changed the number of candidates to 50 and the final samples per target to 25, to speed up the attack process.

A.2 Dataset Details

We state the number of identities and samples for each custom CelebA subset in Appx. A.2. We further state the lowest, median and maximum number of samples of a single identity per attribute and for the total dataset. For the filter models, the datasets contained 155,304 samples (gender and eyeglasses) and 93,942 (hair color), respectively.

Attribute	Value	Identities	Total Samples	Min Samples	Median Samples	Max Samples	Avg Samples
CelebA Gender	Female	250	7,639	30	30	35	30.56
	Male	250	7,652	30	30	36	30.61
	Total	500	15,291	30	30	36	30.58
CelebA Glasses	No Glasses	100	3186	31	32	36	31.86
	Glasses	100	2,346	20	22	31	23.46
	Total	200	5532	20	31	36	27.66
CelebA Race	Asian	100	2944	28	30	31	29.44
	Black	100	2876	26	29	34	28.76
	Indian	100	2281	19	22	30	22.81
	White	100	3164	31	31	35	31.64
	Total	400	11,265	19	29	35	28.16
CelebA Hair Color	Black Hair	100	2,840	23	28	32	28.40
	Blond Hair	100	2,867	25	29	31	28.67
	Brown Hair	100	2,564	17	26	30	25.64
	Gray Hair	100	2,117	14	20	31	21.17
	Total	400	10,388	14	27	32	25.97
FaceScrub Gender	Female	265	17,743	9	65	140	66.95
	Male	265	20,136	25	77	128	75.98
	Total	530	37,879	9	72	140	71.47

Table 2: Dataset identity statistics

A.3 Training Hyperparameters

We emphasize that we did not aim for achieving state-of-the-art performances but rather tried to train models with generally good prediction performance. All non-robust models were initialized with pre-trained ImageNet weights and trained for 80 epochs with an initial learning rate of 0.1 and a batch size of 128. We multiplied the learning rate by factor 0.1 after 60 and 70 epochs. For the models trained with adversarial training, set the number of epochs to 100 and reduced the learning rate after 80 and 90 epochs. Optimization was done with SGD and a momentum of 0.9. Images were resized to 224×224 and normalized with $\mu = \sigma = 0.5$ to set the pixel value range to $[-1, 1]$. As augmentation, we applied random horizontal flipping with $p = 0.5$ flipping probability and random resized cropping with scale $= [0.8, 1.0]$ and ratio $= [0.8, 1.25]$. Cropped images were resized to size 224×224 . Due to the limited number of training samples available for each identity, we did not use a validation set and early stopping. For each architecture and dataset, we trained three models with different seeds. Performance evaluation was done on a holdout test set.

We further trained ResNet-50 models on the CelebA attributes for gender, eyeglasses, and hair color for filtering the candidate images. All models were initialized with pre-trained ImageNet weights and trained for 10 epochs with an initial learning rate of $1e - 3$ and a batch size of 128. We multiplied the learning rate by factor 0.1 after 9 epochs. We used the Adam optimizer [31] with $\beta = (0.9, 0.999)$ and no weight decay. Normalization and augmentation were identical to training the target models, except the scale and ratio parameters of the random resized cropping, which we set to $[0.9, 1.0]$ and $[1.0, 1.0]$ to prevent cutting out the attributes from the training samples. We again used no validation set for early stopping. To calibrate the models, we applied label smoothing with smoothing factor $\alpha = 0.1$ during training. Since some attributes are more frequent in the CelebA dataset, we draw the same number of samples for each attribute by oversampling / undersampling from the attribute images. Details on the training of FairFace for filtering the racial appearance images can be found at <https://github.com/dchen236/FairFace>.

Dataset	Num Classes	Architecture	Accuracy
Gender	500	ResNet-18	$85.99\% \pm 0.21$
		ResNet-101	$86.78\% \pm 0.66$
		ResNet-152	$86.62\% \pm 0.62$
		DenseNet-169	$75.93\% \pm 5.54$
		ResNeSt-101	$81.53\% \pm 4.40$
Eyeglasses	200	ResNet-18	$93.08\% \pm 0.58$
		ResNet-101	$90.97\% \pm 1.41$
		ResNet-152	$91.10\% \pm 0.85$
		DenseNet-169	$93.56\% \pm 0.38$
		ResNeSt-101	$90.73\% \pm 0.21$
Race	400	ResNet-18	$84.65\% \pm 0.44$
		ResNet-101	$82.99\% \pm 0.40$
		ResNet-152	$84.06\% \pm 1.19$
		DenseNet-169	$85.00\% \pm 0.96$
		ResNeSt-101	$81.13\% \pm 1.04$
Hair Color	400	ResNet-18	$87.94\% \pm 0.56$
		ResNet-101	$87.65\% \pm 0.70$
		ResNet-152	$87.20\% \pm 0.67$
		DenseNet-169	$88.45\% \pm 1.68$
		ResNeSt-101	$85.53\% \pm 0.53$

(a) CelebA

Dataset	Num Classes	Architecture	Accuracy
FaceScrub Cropped	530	ResNet-18	$93.92\% \pm 0.17$
		ResNet-101	$94.93\% \pm 0.43$
		ResNet-152	$95.32\% \pm 0.22$
		DenseNet-169	$91.93\% \pm 0.65$
		ResNeSt-101	$93.50\% \pm 0.70$
FaceScrub Cropped Robust	530	ResNet-18	$83.79\% \pm 0.21$
		ResNet-101	$88.12\% \pm 0.24$
		ResNet-152	$87.11\% \pm 0.28$
		DenseNet-169	$88.53\% \pm 0.76$
		ResNeSt-101	$90.04\% \pm 0.48$
FaceScrub Uncropped	530	ResNet-18	$70.29\% \pm 2.71$
		ResNet-101	$78.75\% \pm 0.84$
		ResNet-152	$78.52\% \pm 0.58$
		DenseNet-169	$69.11\% \pm 12.73$
		ResNeSt-101	$77.32\% \pm 0.54$
FaceScrub Uncropped Robust	530	ResNet-18	$41.58\% \pm 0.63$
		ResNet-101	$55.23\% \pm 0.60$
		ResNet-152	$55.69\% \pm 1.24$
		DenseNet-169	$54.65\% \pm 2.98$
		ResNeSt-101	$58.74\% \pm 0.84$

(b) FaceScrub

Table 3: Prediction accuracy of the target models on the individual test sets.

A.4 Attack Dataset Generation

To create the attack dataset, we first applied Null-Text Inversion [36] with 50 DDIM steps and a guidance scale of 7.5 on Stable Diffusion v1.5³. We further used the generic prompt “*A photo of a person*” for all samples. After the inversion, we generated image variations by adding the sensitive attribute values to the prompt using prompt-to-prompt, e.g., “*A photo of a person, female appearance*” and “*A photo of a person, male appearance*” to generate gender variations. We set the cross replace steps to 1.0 and the self replace steps to 0.4 for gender and eyeglasses, and to 0.6 for hair color and racial appearance. The confidence threshold for the filter models was set to 0.6 for all models. We then generated and filtered attribute variations one after another, until we collected 300 candidates for each attribute category. Tab. 1 states all prompts used for generating.

Attribute	Value	Prompt
Gender	Female	<i>female appearance</i>
	Male	<i>male appearance</i>
Glasses	No Glasses	<i>no eyeglasses</i>
	Glasses	<i>wearing eyeglasses</i>
Racial Appearance	Asian	<i>with asian appearance</i>
	Black	<i>with black skin</i>
	Indian	<i>with indian appearance</i>
	White	<i>with white skin</i>
Hair Color	Black	<i>with black hair</i>
	Blond	<i>with blond hair</i>
	Brown	<i>with brown hair</i>
	Gray	<i>with gray hair</i>

Table 4: Prompts for attack dataset generation. Each prompt is appended to the string “*A photo of a person, ()*” by replacing () with the attribute-specific prompt.

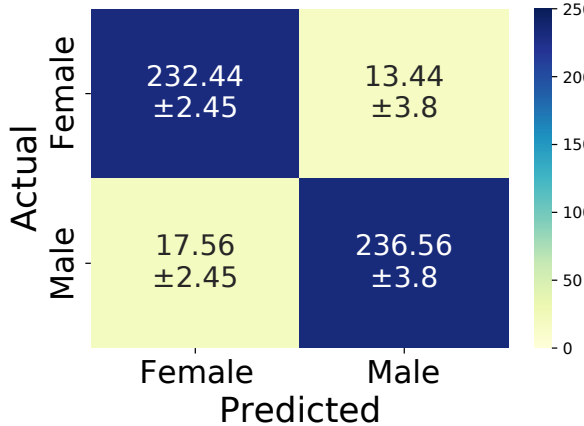
Attribute	Num Classes	Training Samples	Architecture	Accuracy
Gender	2	155,304	ResNet-50	98.98%
Glasses	2	155,304	ResNet-50	98.81%
Hair Color	4	93,940	ResNet-50	93.51%

Table 5: Prediction accuracy of the filter models on the individual test sets.

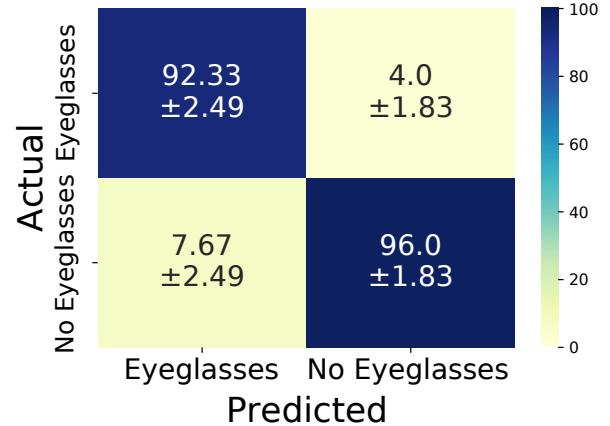
³Available at <https://huggingface.co/runwayml/stable-diffusion-v1-5>.

B Additional CelebA Experimental Results

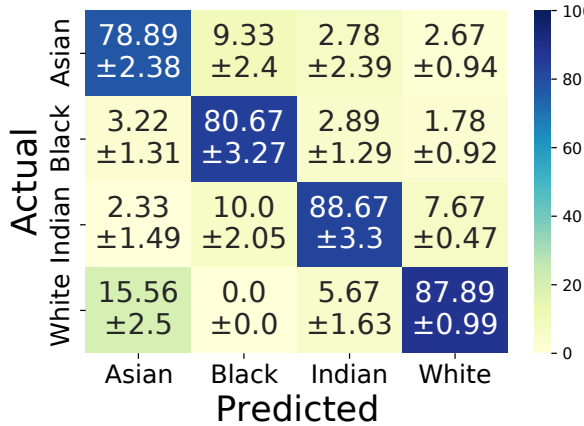
B.1 Confusion Matrices for CelebA ResNet-101 Models



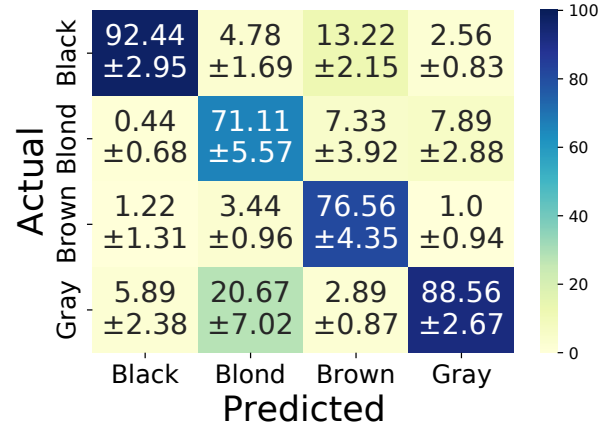
(a) Gender (FFHQ)



(b) Eyeglasses (FFHQ)



(c) Racial Appearance (FFHQ)



(d) Hair Color (FFHQ)

Figure 12: Confusion Matrices for ResNet-101 models trained on the four different CelebA subsets. All attacks were performed against three target models and with three different attack datasets.

B.2 ResNet-18 - CelebA

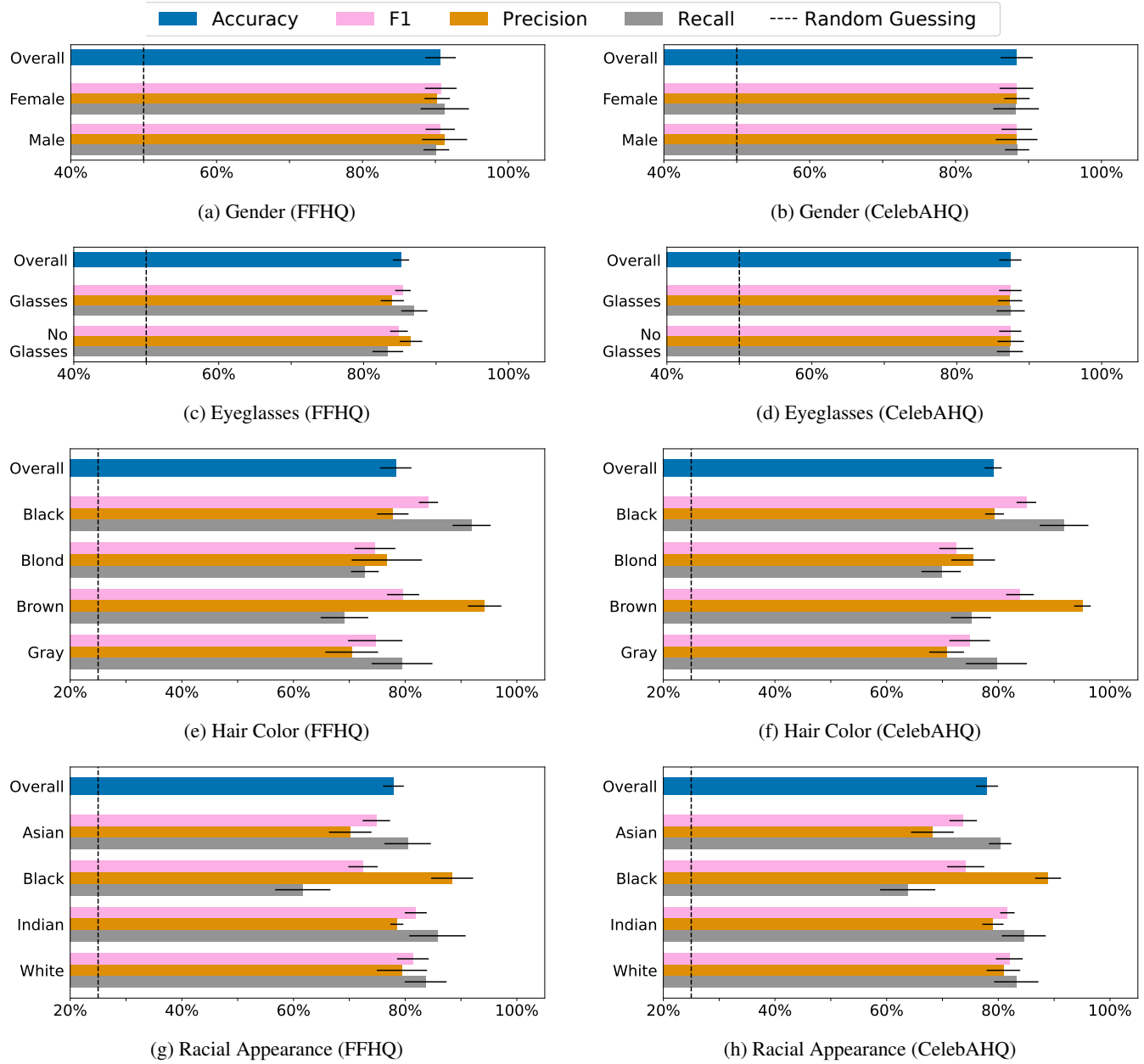


Figure 13: Evaluation results for CAIA performed on ResNet-18 models to infer four different target attributes. The black horizontal lines denote the standard deviation over nine runs. We further state random guessing (dashed line) for comparison.

B.3 ResNet-18 - CelebA (1000 Targets)

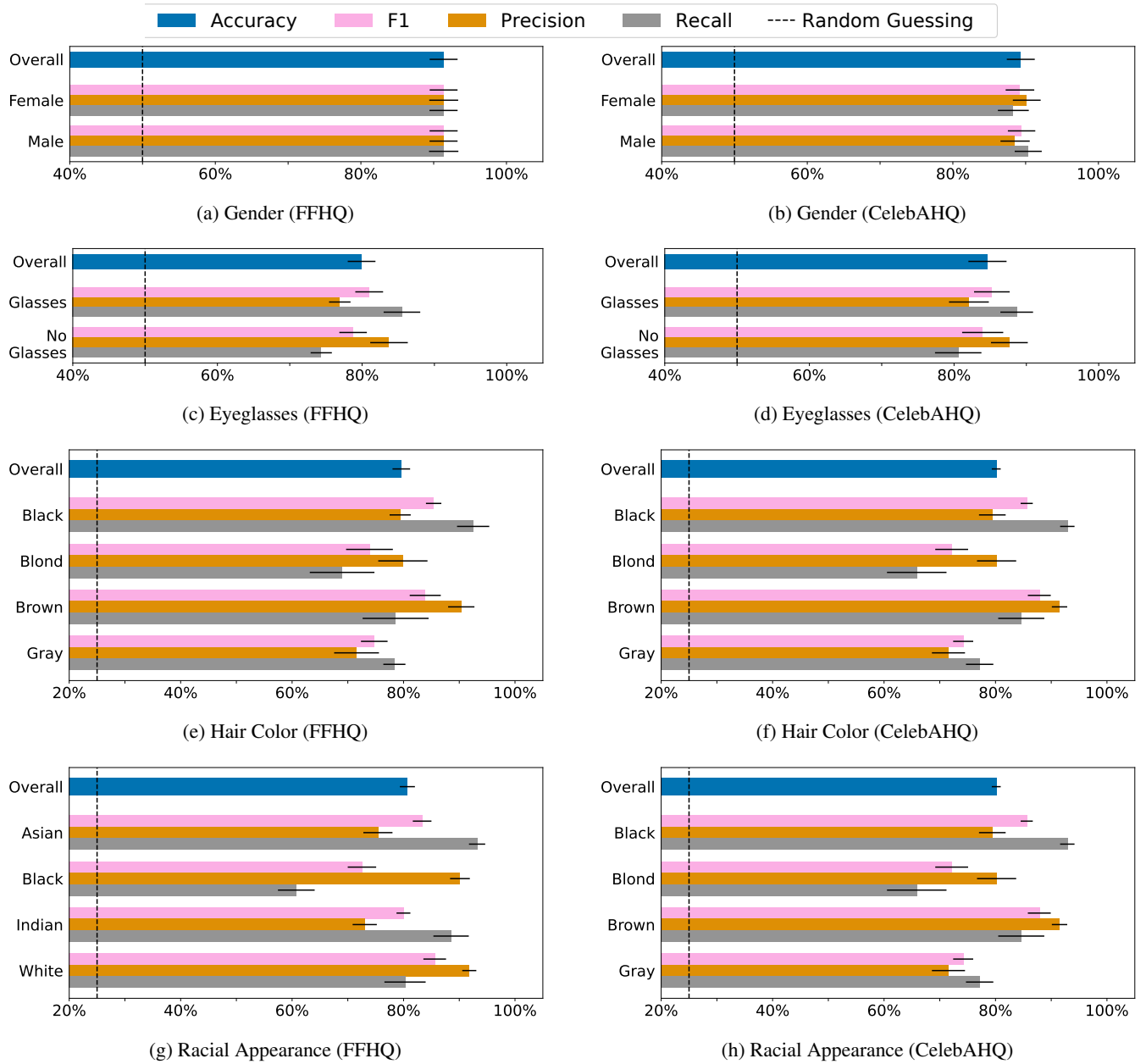


Figure 14: Evaluation results for CAIA performed on ResNet-18 models to infer four different target attributes and **1000** identities. The black horizontal lines denote the standard deviation over nine runs. We further state random guessing (dashed line) for comparison.

B.4 ResNet-101 - CelebA

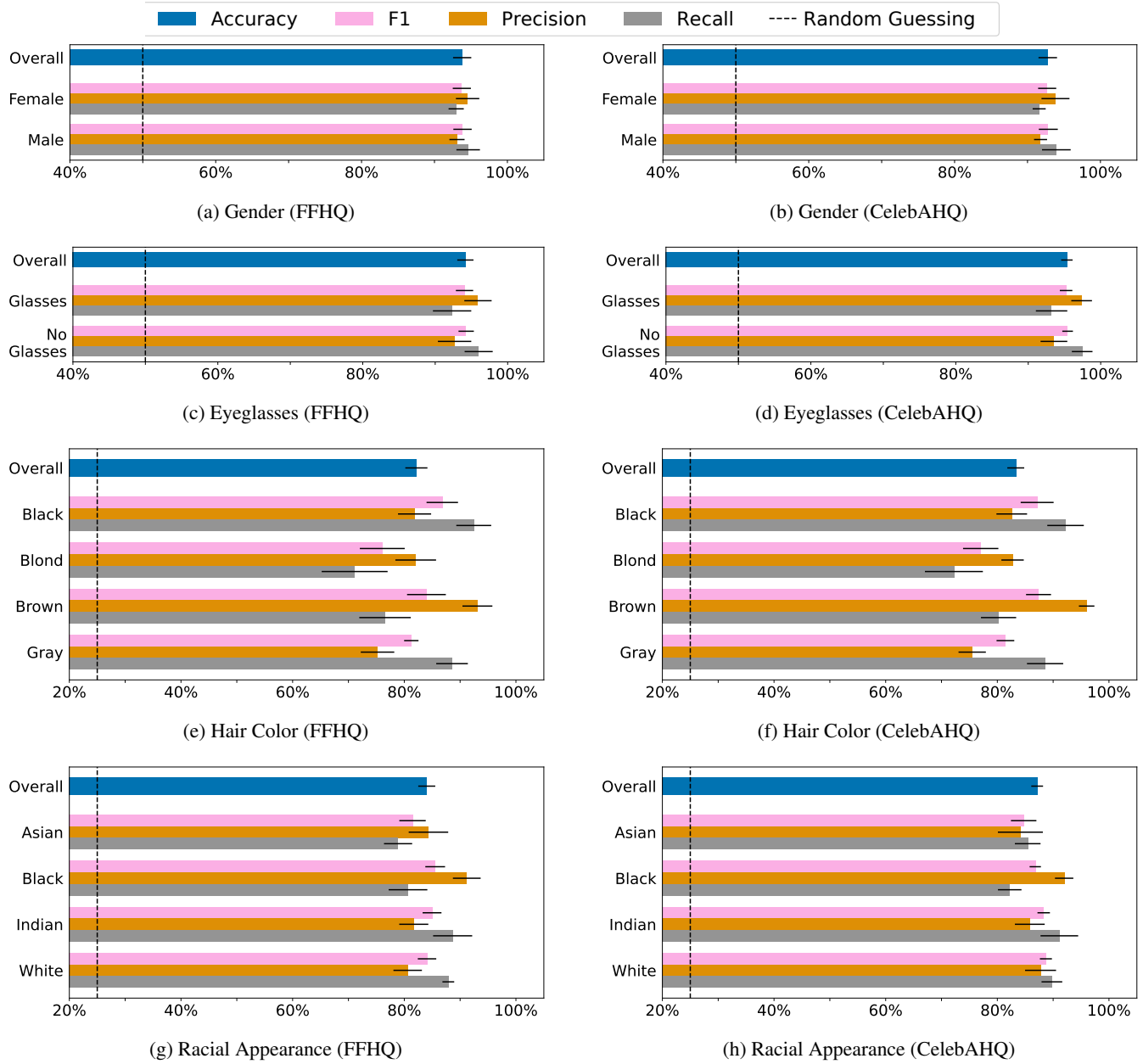


Figure 15: Evaluation results for CAIA performed on ResNet-101 models to infer four different target attributes. The black horizontal lines denote the standard deviation over nine runs. We further state random guessing (dashed line) for comparison.

B.5 ResNet-101 - CelebA (1000 identities)

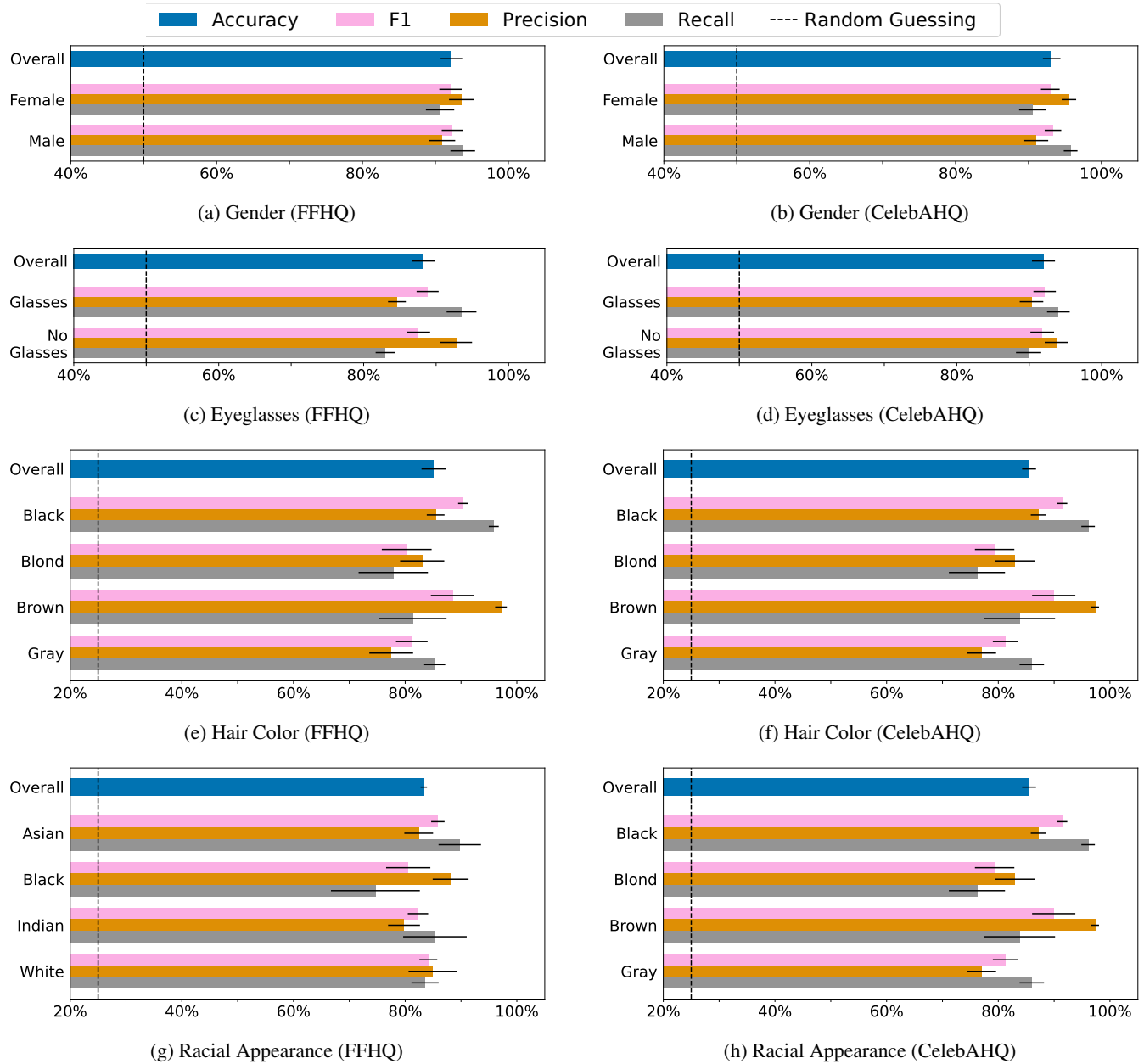


Figure 16: Evaluation results for CAIA performed on ResNet-101 models to infer four different target attributes for **1000** identities. The black horizontal lines denote the standard deviation over nine runs. We further state random guessing (dashed line) for comparison.

B.6 ResNet-152 - CelebA

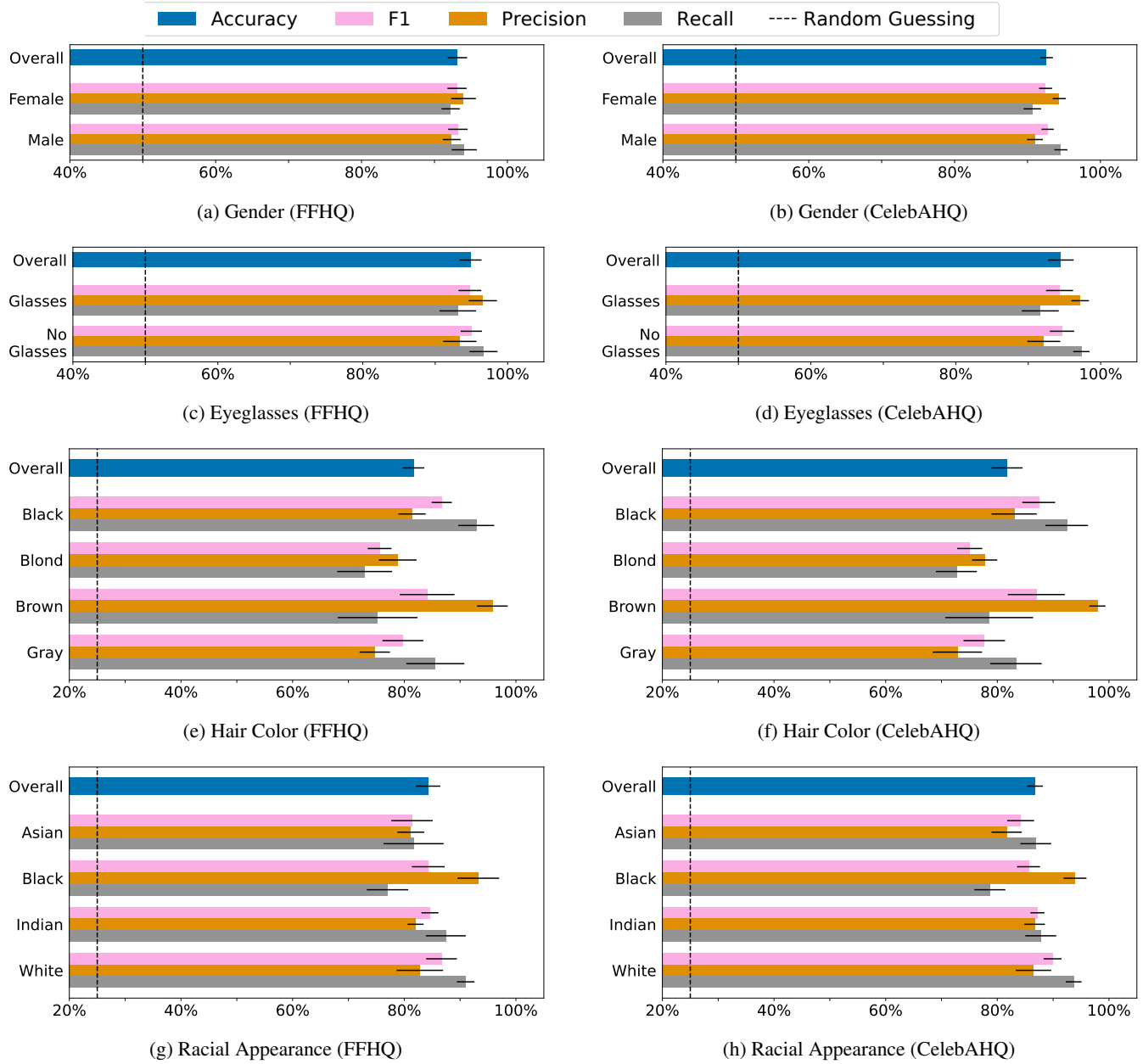


Figure 17: Evaluation results for CAIA performed on ResNet-152 models to infer four different target attributes. The black horizontal lines denote the standard deviation over nine runs. We further state random guessing (dashed line) for comparison.

B.7 ResNet-152 - CelebA (1000 identities)

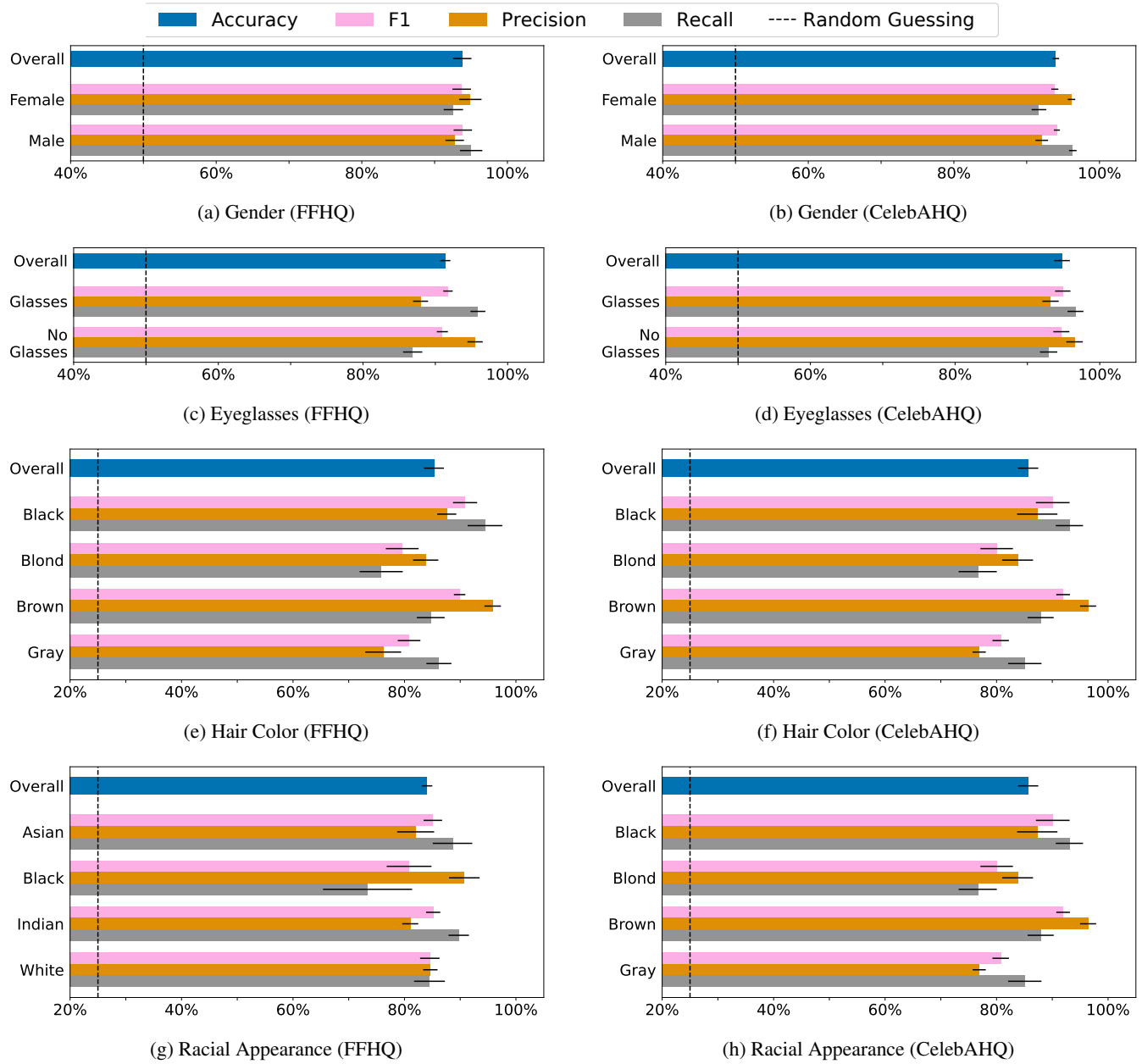


Figure 18: Evaluation results for CAIA performed on ResNet-152 models to infer four different target attributes for **1000** identities. The black horizontal lines denote the standard deviation over nine runs. We further state random guessing (dashed line) for comparison.

B.8 DenseNet-169 - CelebA

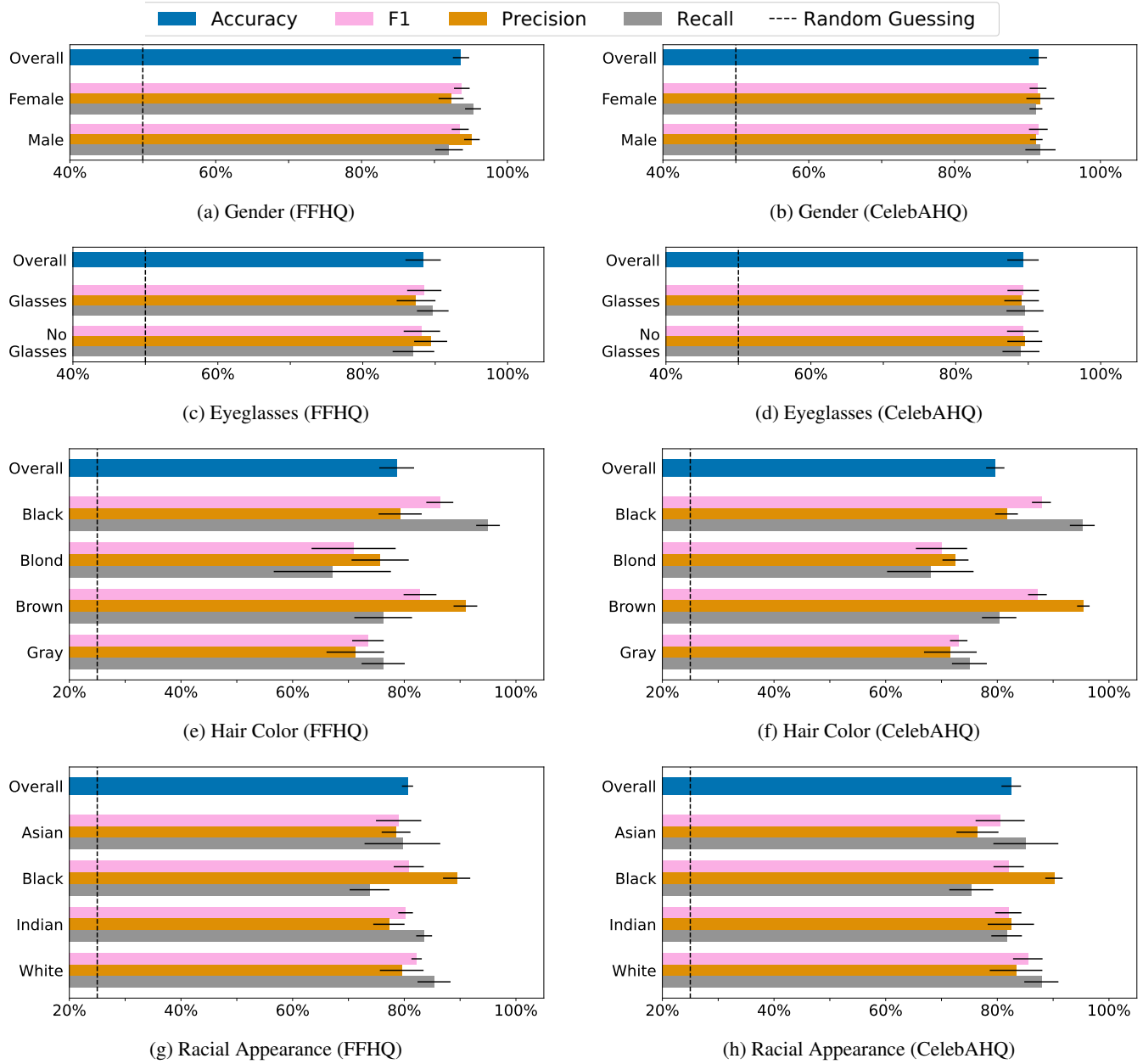


Figure 19: Evaluation results for CAIA performed on DenseNet-169 models to infer four different target attributes. The black horizontal lines denote the standard deviation over nine runs. We further state random guessing (dashed line) for comparison.

B.9 DenseNet-169 - CelebA (1000 identities)

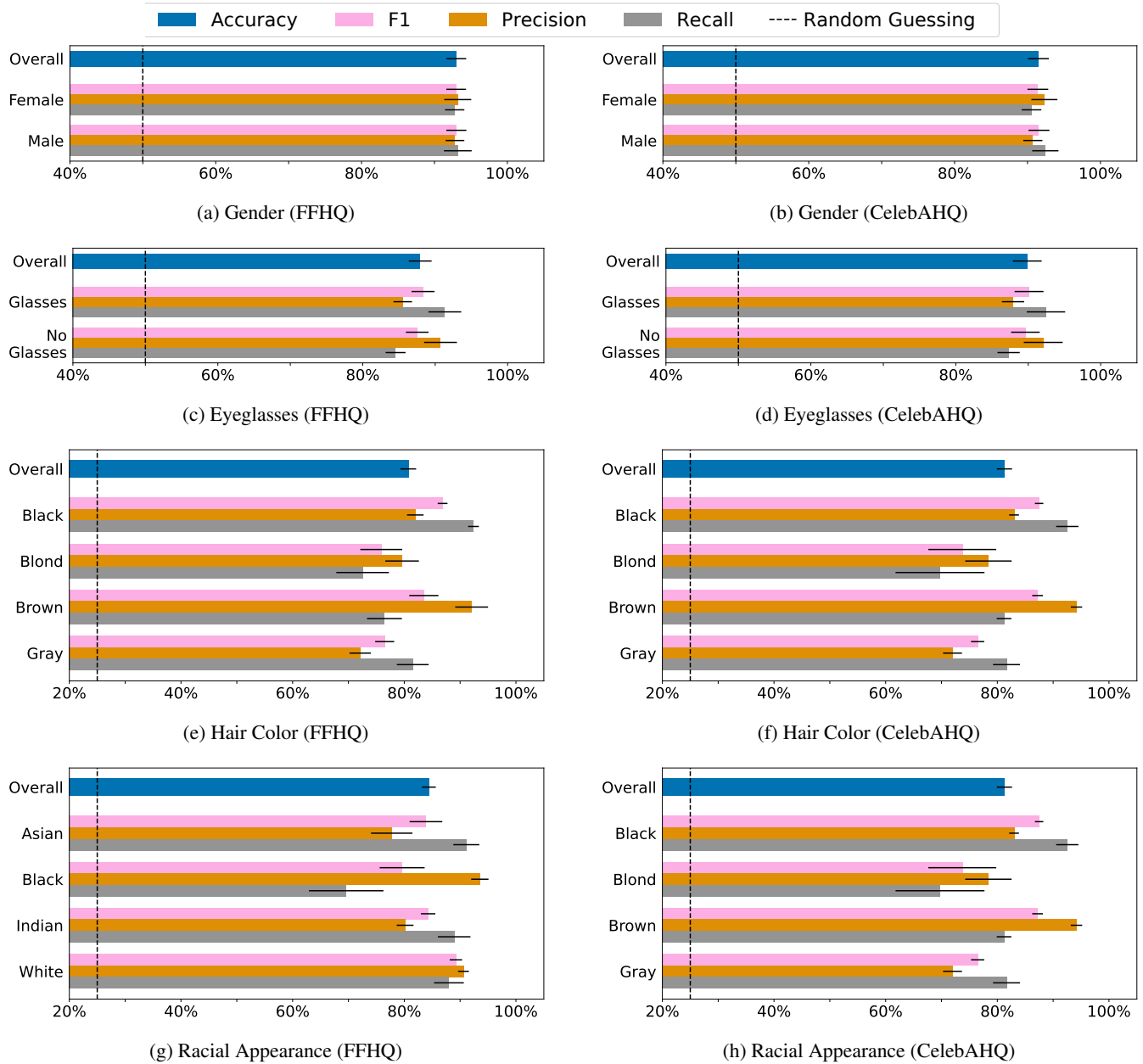


Figure 20: Evaluation results for CAIA performed on DenseNet-169 models to infer four different target attributes for **1000** identities. The black horizontal lines denote the standard deviation over nine runs. We further state random guessing (dashed line) for comparison.

B.10 ResNeSt-101 - CelebA

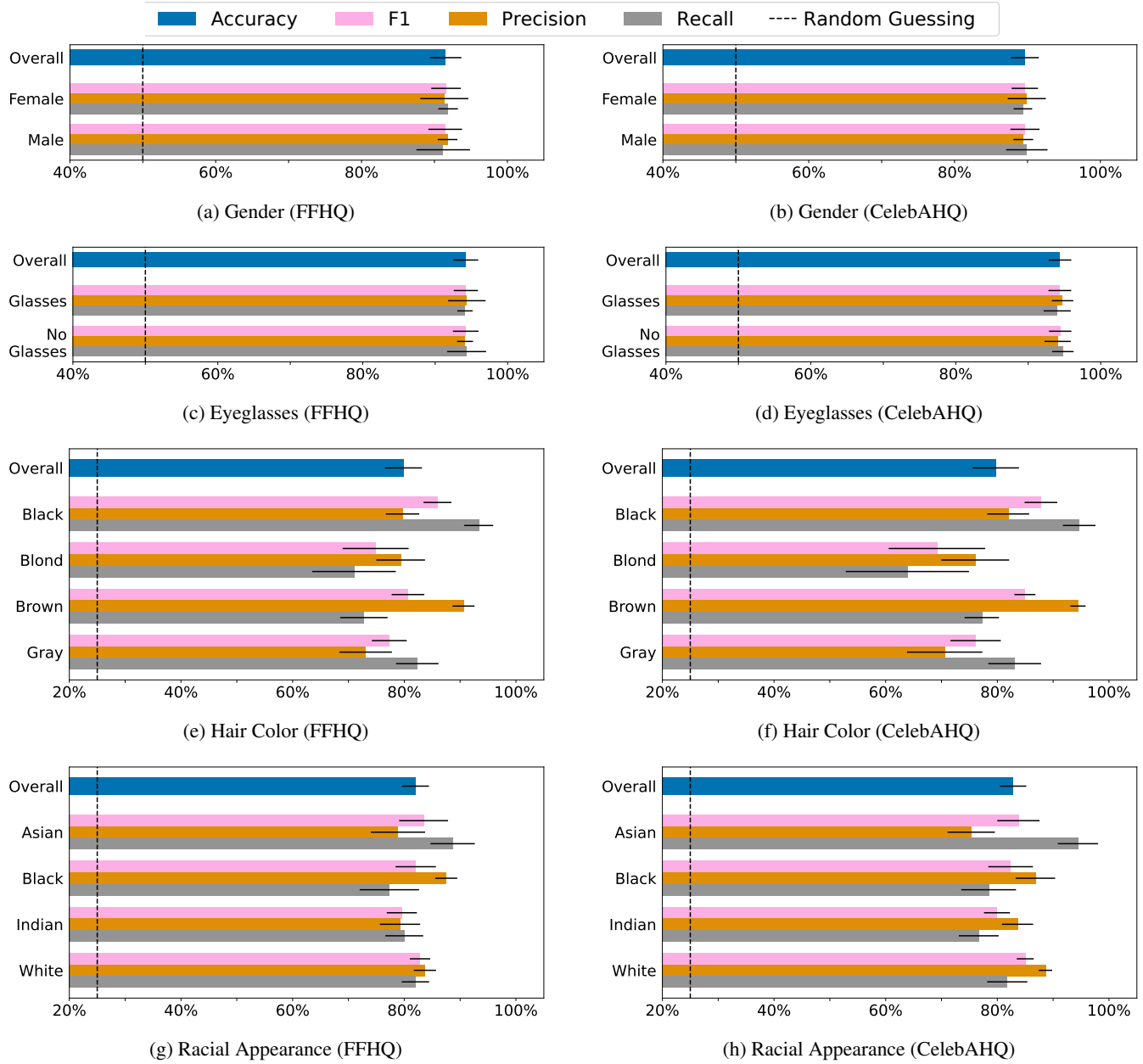


Figure 21: Evaluation results for CAIA performed on ResNeSt-101 models to infer four different target attributes. The black horizontal lines denote the standard deviation over nine runs. We further state random guessing (dashed line) for comparison.

B.11 ResNeSt-101 - CelebA (1000 identities)

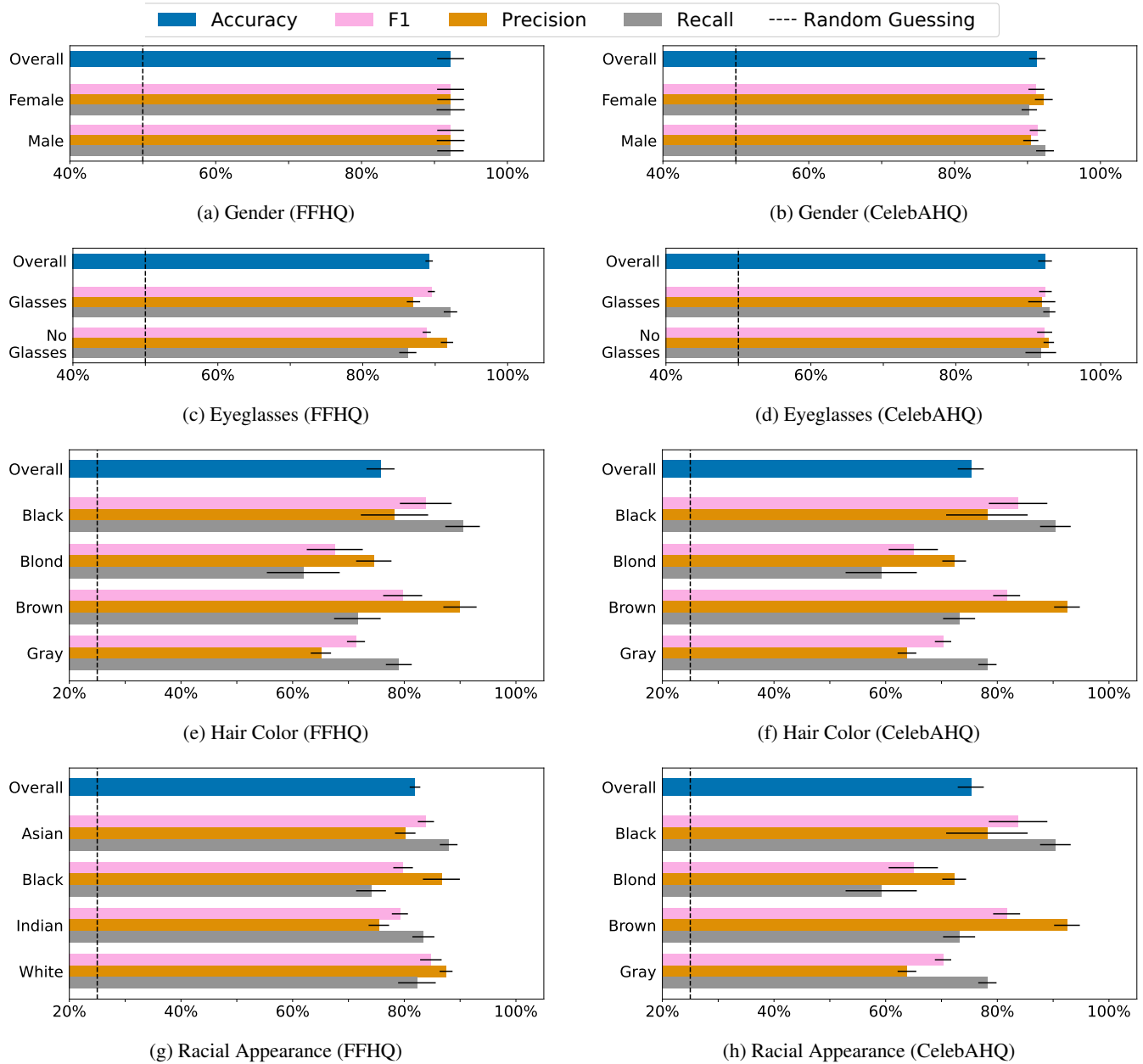


Figure 22: Evaluation results for CAIA performed on ResNeSt-101 models to infer four different target attributes for **1000** identities. The black horizontal lines denote the standard deviation over nine runs. We further state random guessing (dashed line) for comparison.

C Additional FaceScrub Experimental Results

C.1 ResNet-18 - FaceScrub (Cropped)

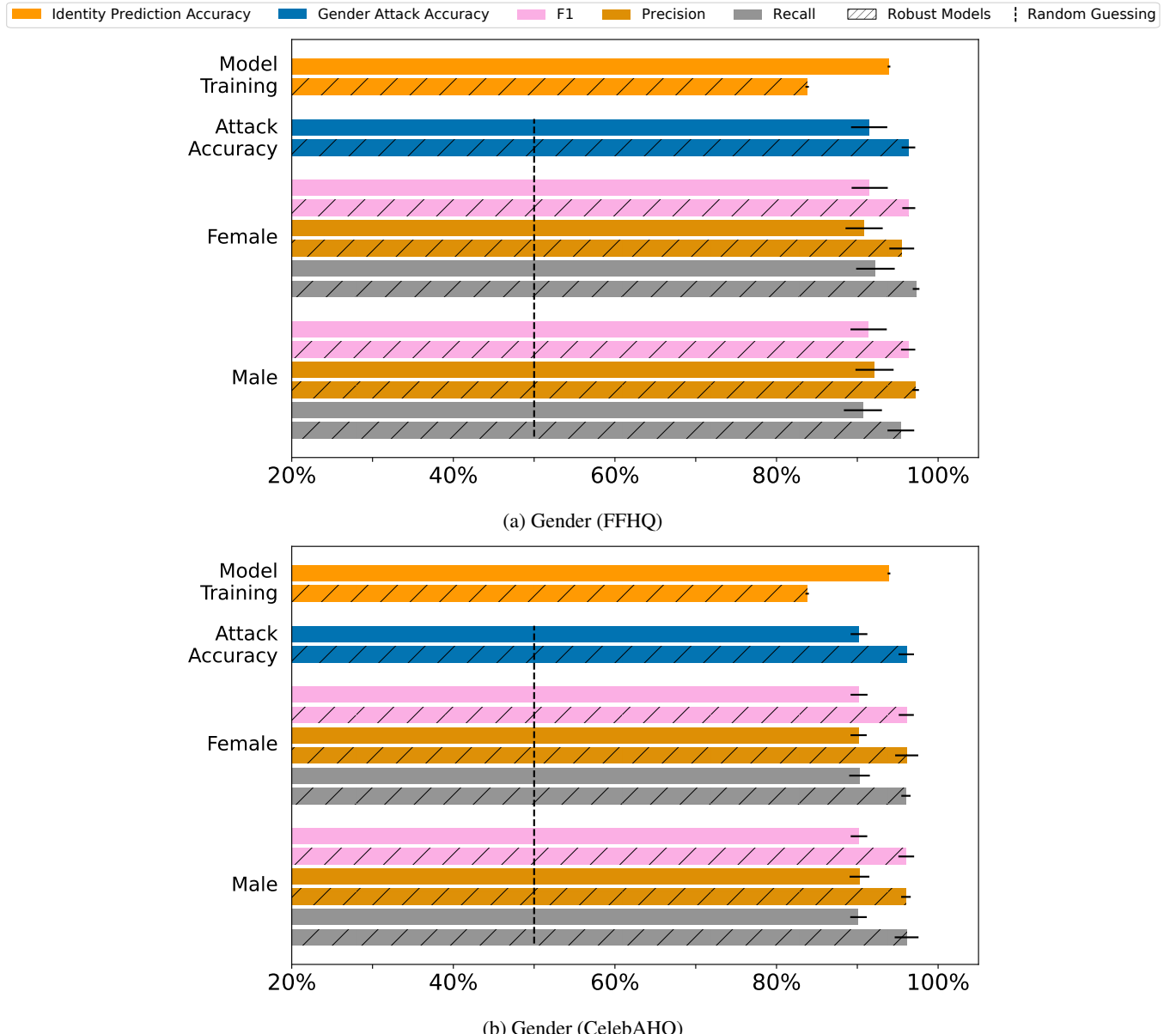


Figure 23: Evaluation results for CAIA performed on ResNet-18 models to infer the gender appearance. The black horizontal lines denote the standard deviation over nine runs. We further state random guessing (dashed line) for comparison. The models were trained on the cropped FaceScrub dataset.

C.2 ResNet-101 - FaceScrub (Cropped)

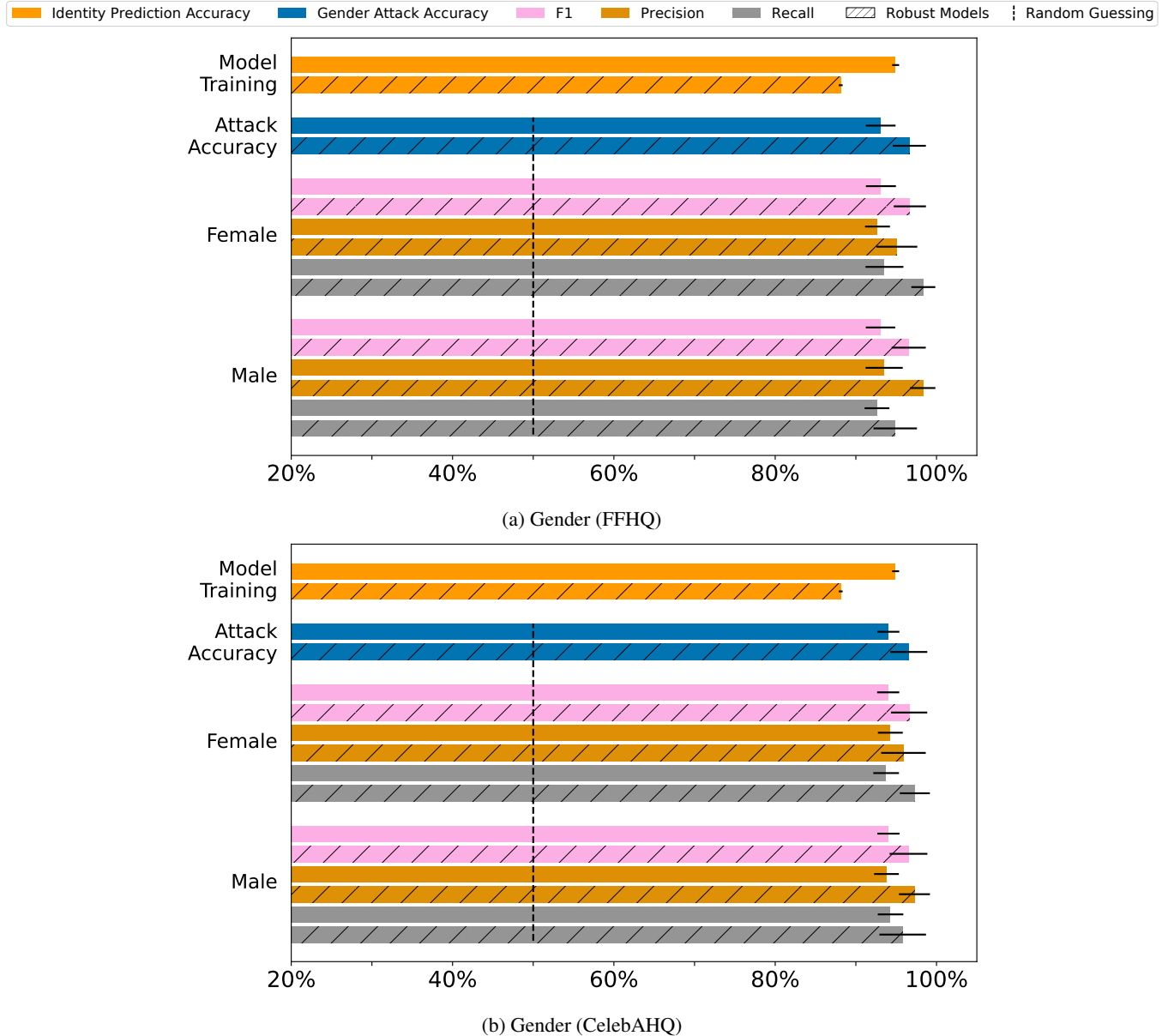


Figure 24: Evaluation results for CAIA performed on ResNet-101 models to infer the gender appearance. The black horizontal lines denote the standard deviation over nine runs. We further state random guessing (dashed line) for comparison. The models were trained on the cropped FaceScrub dataset.

C.3 ResNet-152 - FaceScrub (Cropped)

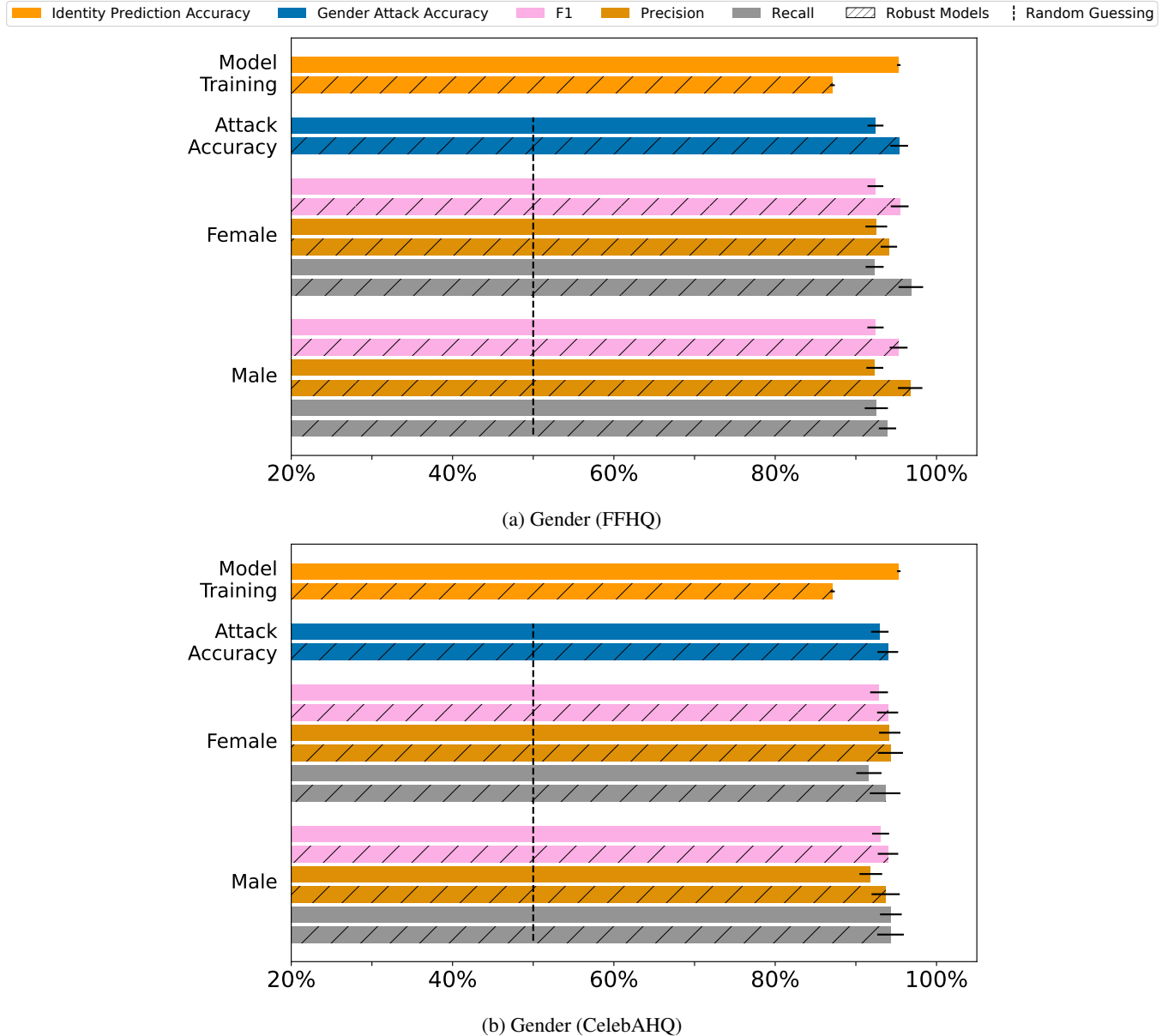


Figure 25: Evaluation results for CAIA performed on ResNet-152 models to infer the gender appearance. The black horizontal lines denote the standard deviation over nine runs. We further state random guessing (dashed line) for comparison. The models were trained on the cropped FaceScrub dataset.

C.4 DenseNet-169 - FaceScrub (Cropped)

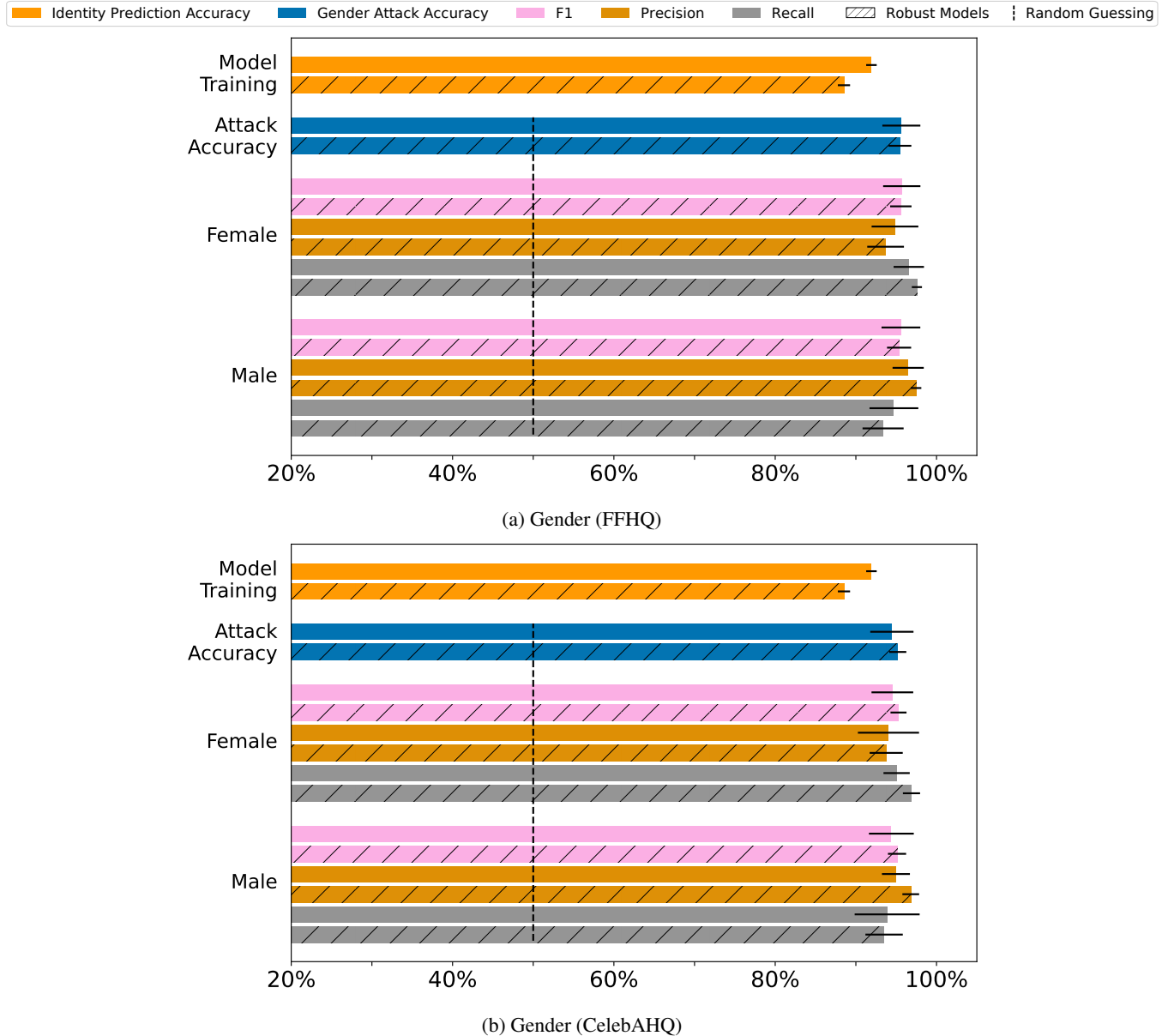


Figure 26: Evaluation results for CAIA performed on DenseNet-169 models to infer the gender appearance. The black horizontal lines denote the standard deviation over nine runs. We further state random guessing (dashed line) for comparison. The models were trained on the cropped FaceScrub dataset.

C.5 ResNeSt-101 - FaceScrub (Cropped)

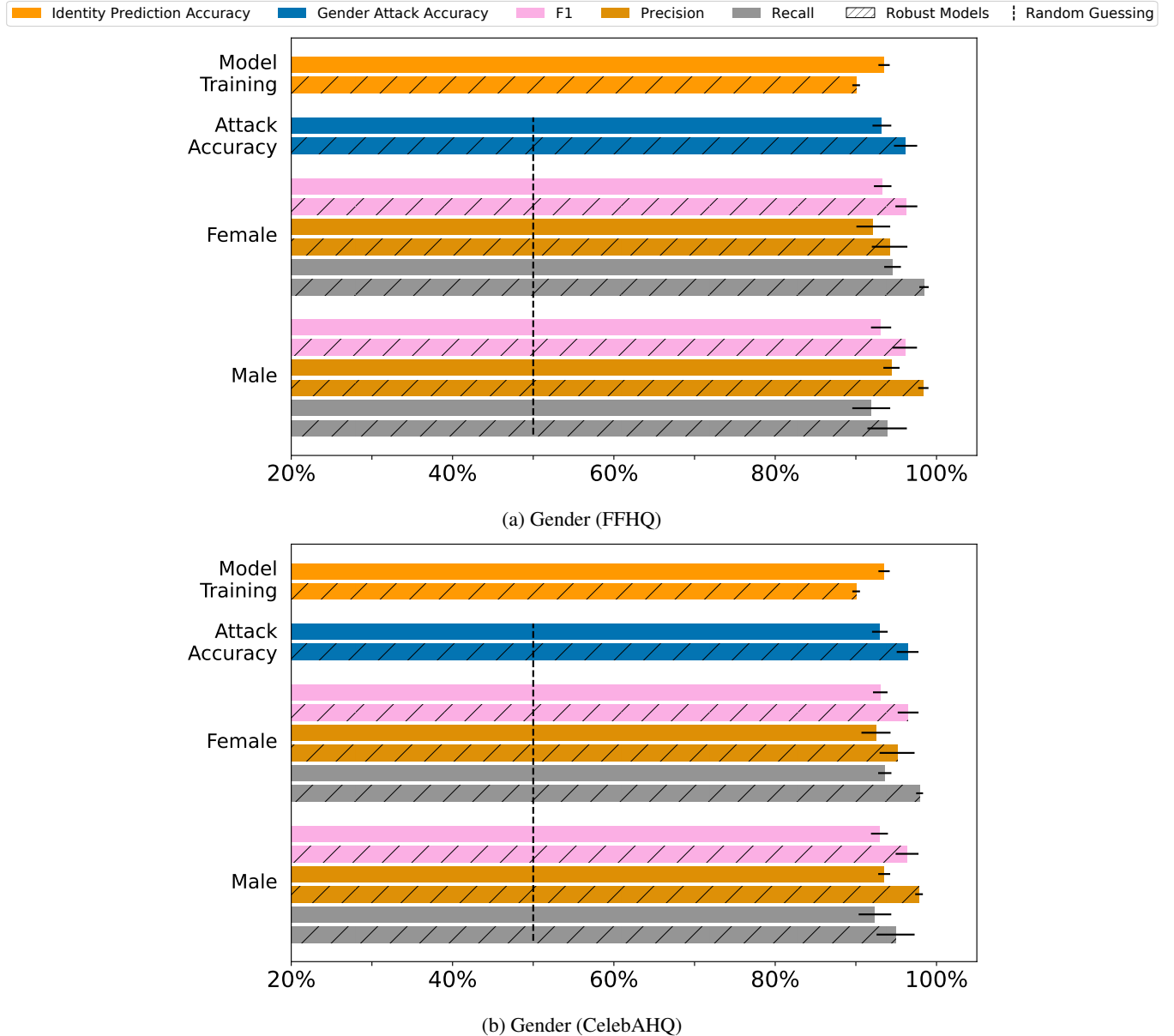


Figure 27: Evaluation results for CAIA performed on ResNeSt-101 models to infer the gender appearance. The black horizontal lines denote the standard deviation over nine runs. We further state random guessing (dashed line) for comparison. The models were trained on the cropped FaceScrub dataset.

C.6 ResNet-18 - FaceScrub (Uncropped)



Figure 28: Evaluation results for CAIA performed on ResNet-18 models to infer the gender appearance. The black horizontal lines denote the standard deviation over nine runs. We further state random guessing (dashed line) for comparison. The models were trained on the cropped FaceScrub dataset.

C.7 ResNet-101 - FaceScrub (Uncropped)

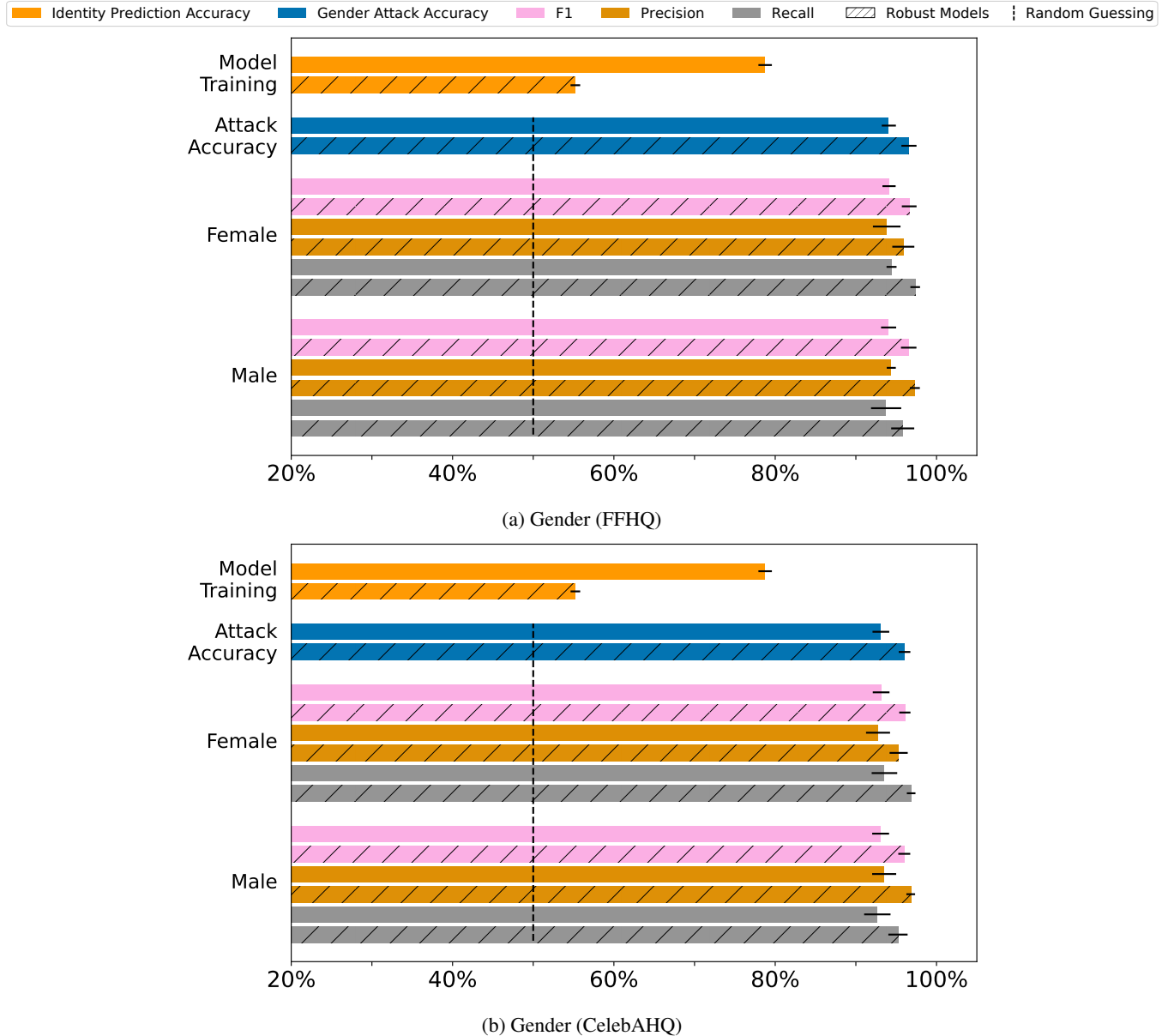


Figure 29: Evaluation results for CAIA performed on ResNet-101 models to infer the gender appearance. The black horizontal lines denote the standard deviation over nine runs. We further state random guessing (dashed line) for comparison. The models were trained on the cropped FaceScrub dataset.

C.8 ResNet-152 - FaceScrub (Uncropped)

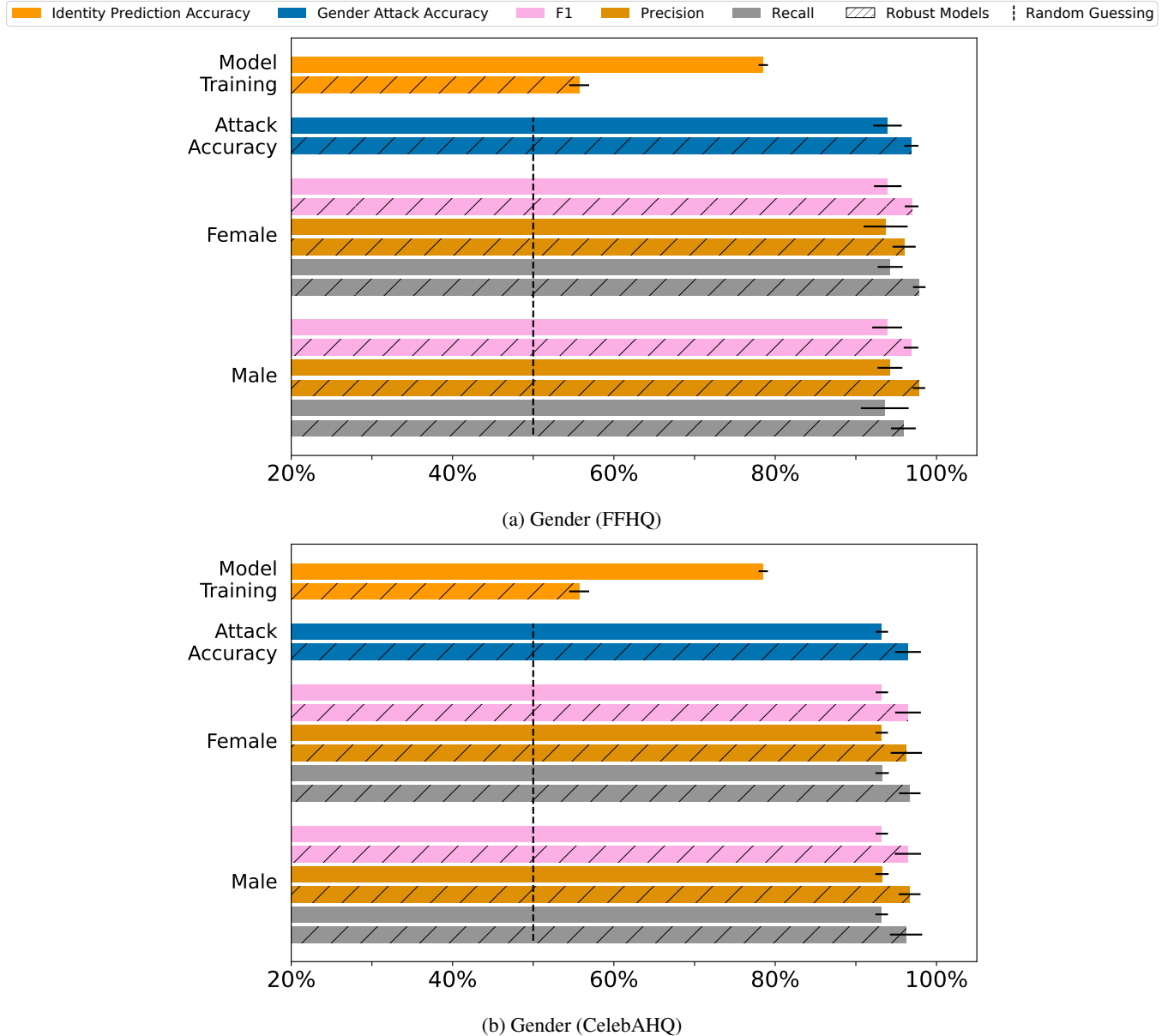


Figure 30: Evaluation results for CAIA performed on ResNet-152 models to infer the gender appearance. The black horizontal lines denote the standard deviation over nine runs. We further state random guessing (dashed line) for comparison. The models were trained on the cropped FaceScrub dataset.

C.9 DenseNet-169 - FaceScrub (Uncropped)

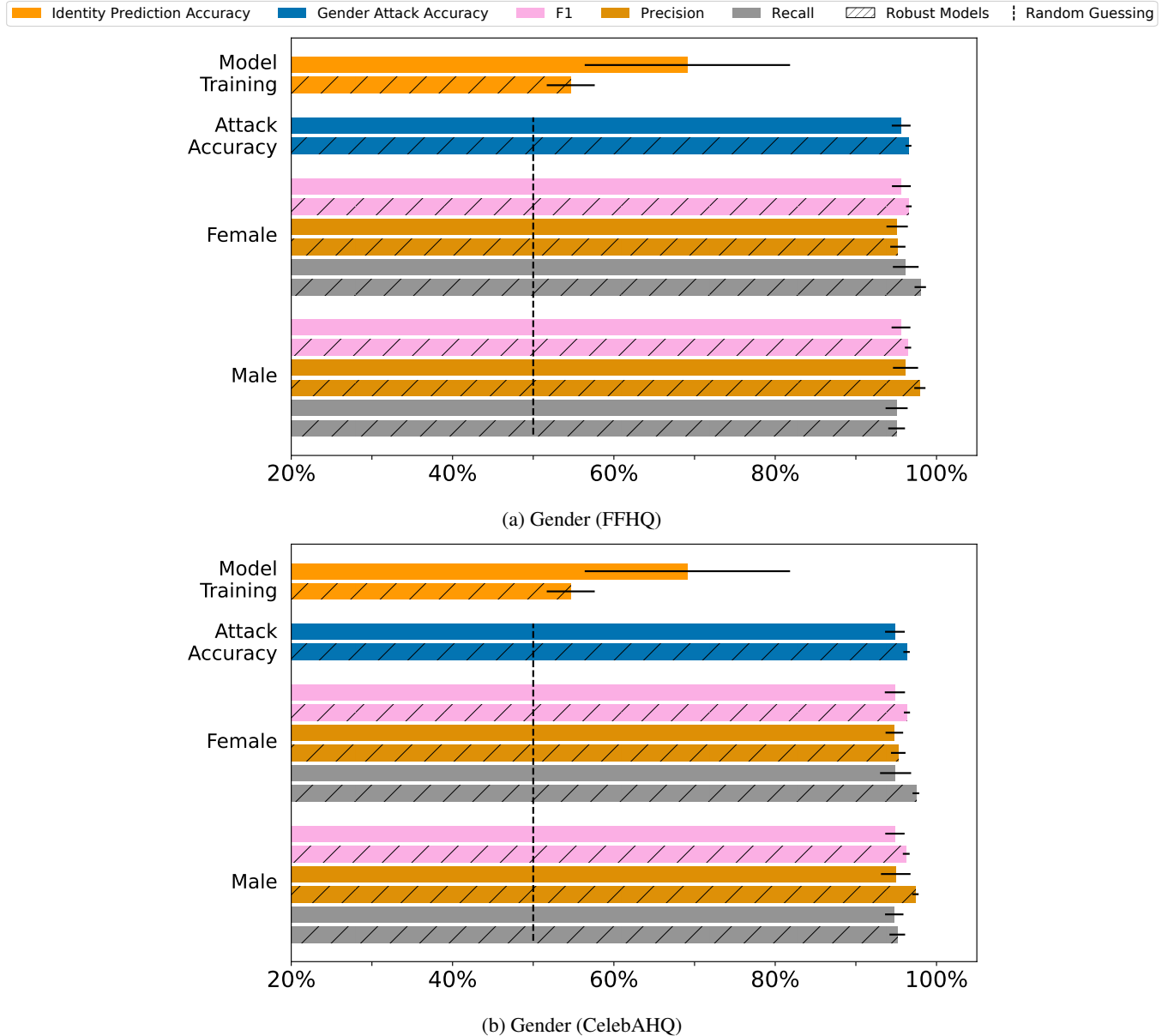


Figure 31: Evaluation results for CAIA performed on DenseNet-169 models to infer the gender appearance. The black horizontal lines denote the standard deviation over nine runs. We further state random guessing (dashed line) for comparison. The models were trained on the cropped FaceScrub dataset.

C.10 ResNeSt-101 - FaceScrub (Uncropped)

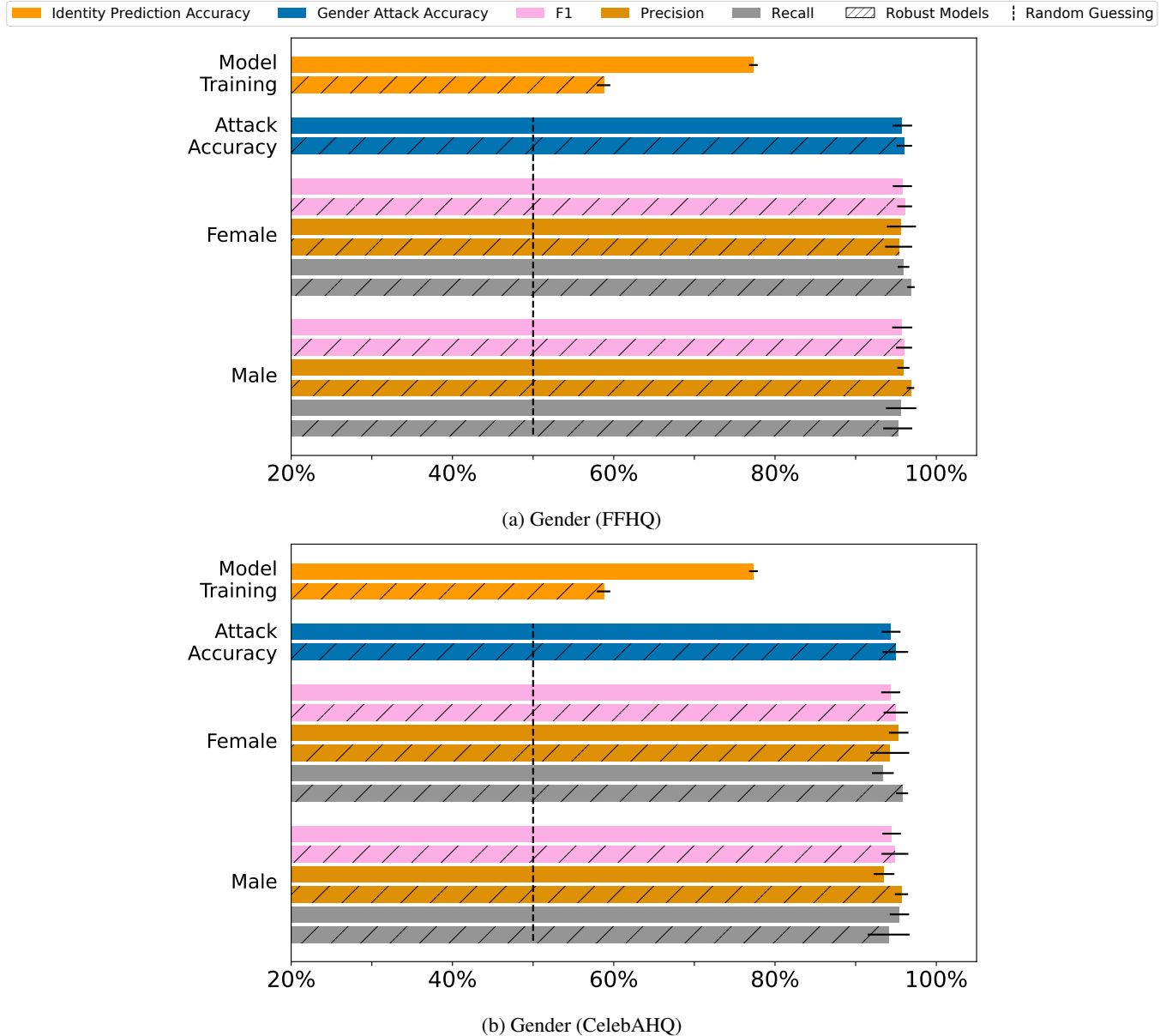


Figure 32: Evaluation results for CAIA performed on ResNeSt-101 models to infer the gender appearance. The black horizontal lines denote the standard deviation over nine runs. We further state random guessing (dashed line) for comparison. The models were trained on the cropped FaceScrub dataset.

D Sample Visualization

D.1 Dataset Samples



Figure 33: Random samples from the different datasets used throughout this work. Note that CelebA and FaceScrub images have much lower resolution than FFHQ and CelebAHQ. Also, the distribution of the images differs significantly.

D.2 Attack Samples for Attribute Gender

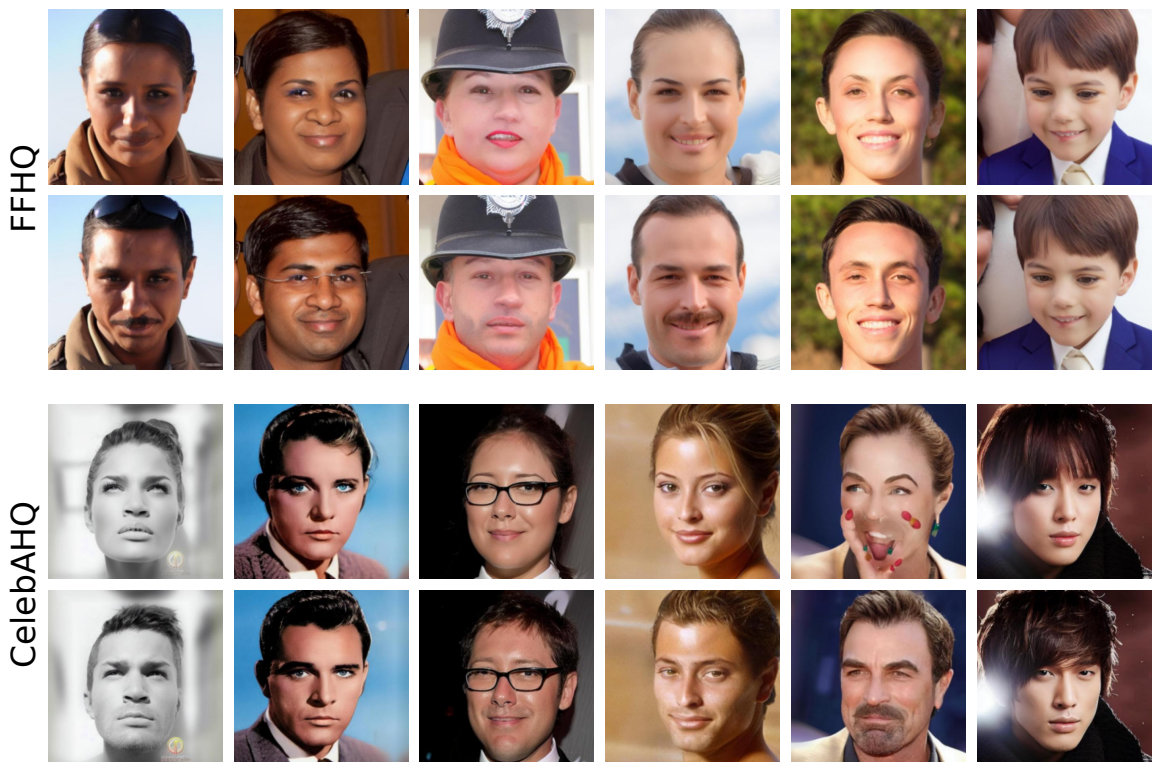


Figure 34: Attack samples to infer the attribute *Gender*.

D.3 Attack Samples for Attribute Eyeglasses



Figure 35: Attack samples to infer the attribute *Eyeglasses*.

D.4 Attack Samples for Attribute Hair Color

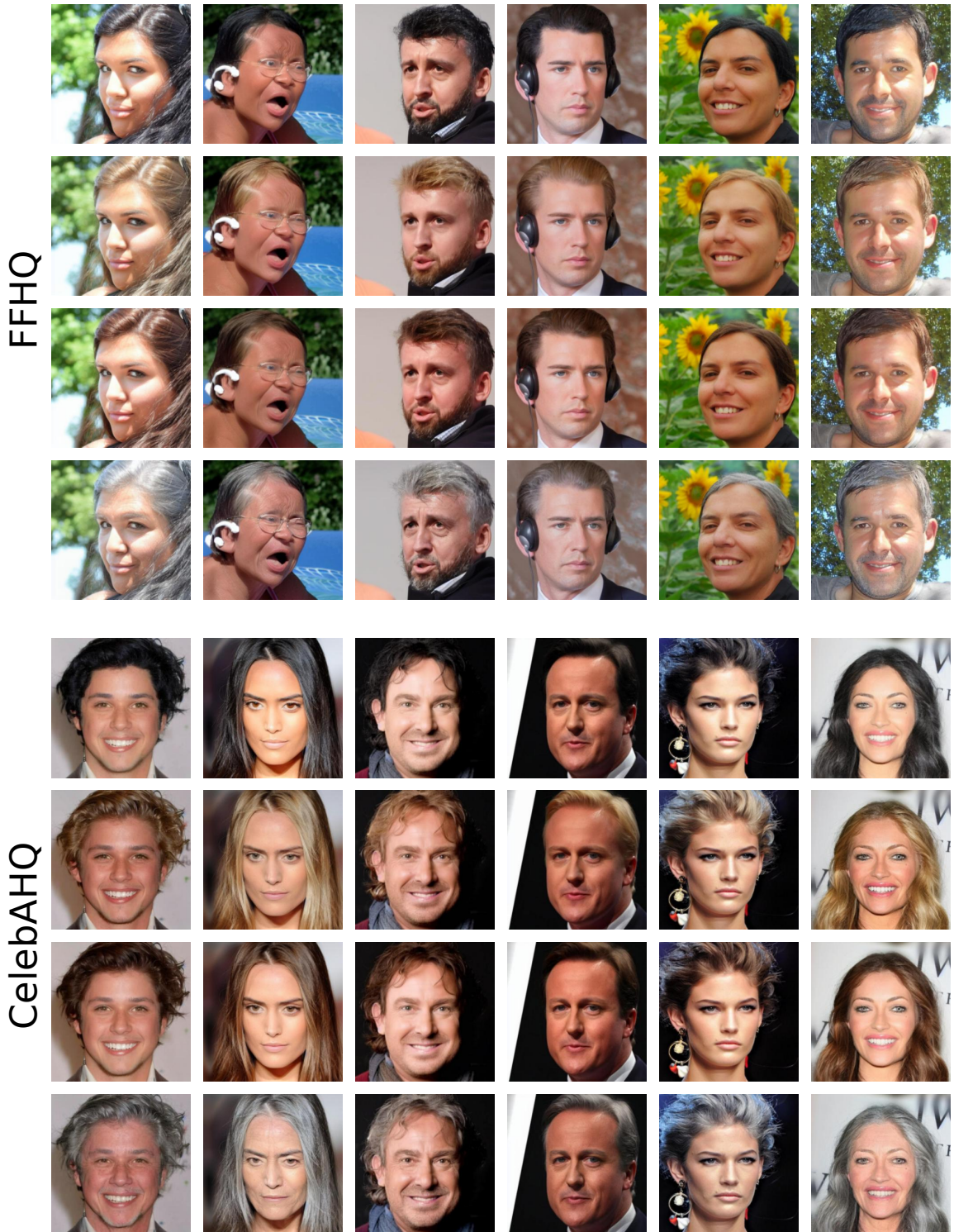


Figure 36: Attack samples to infer the attribute *Hair Color*.

D.5 Attack Samples for Attribute Racial Appearance

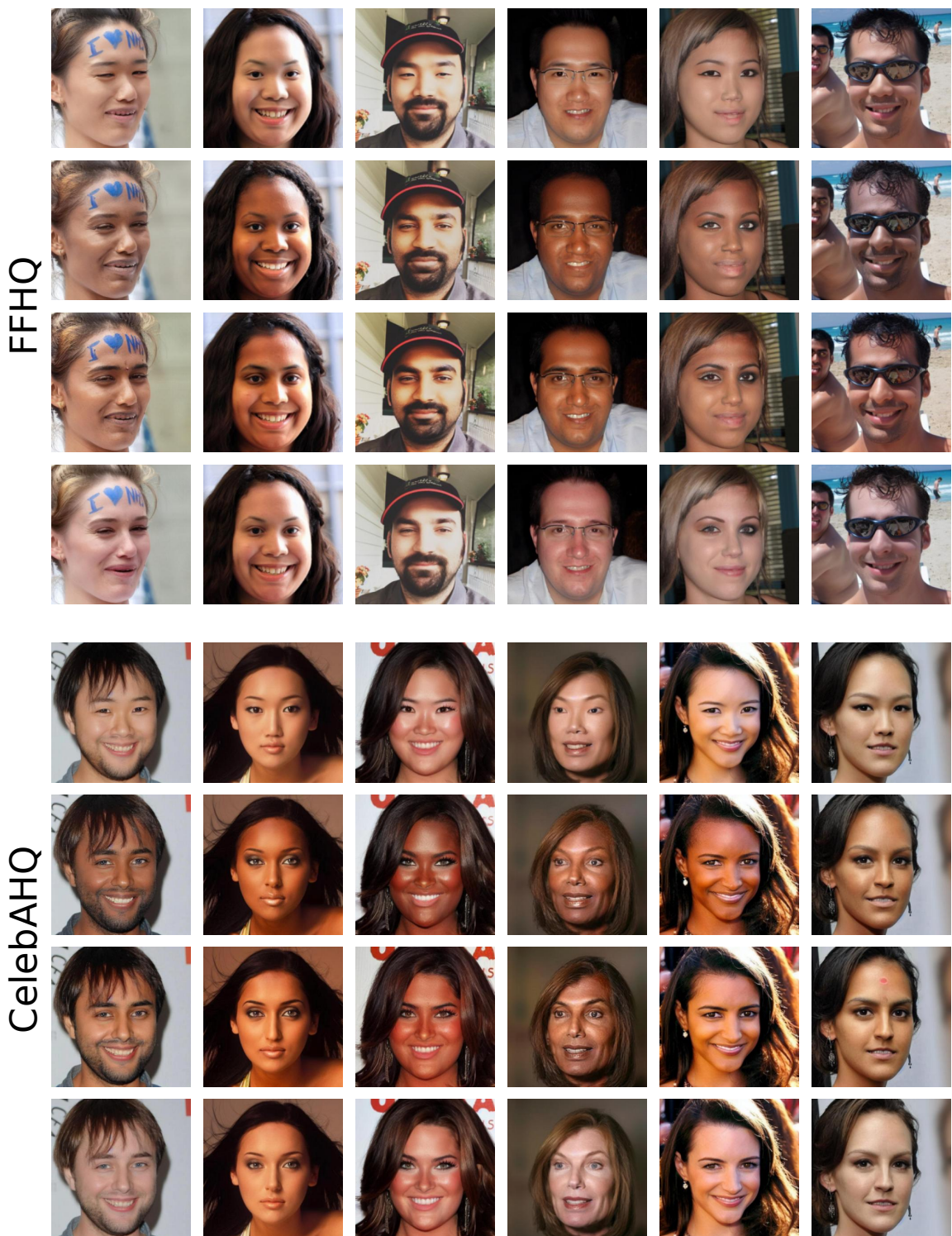


Figure 37: Attack samples to infer the attribute *Racial Appearance*.